Andreia Filipa Nunes de Melo

PHOTODYNAMIC THERAPY WITH GLYCOCONJUGATED PORPHYRINS FOR AGE-RELATED MACULAR DEGENERATION

Dissertation presented to University of Coimbra as a requirement for the degree of MSc in Chemistry, area of specialization in Advanced and Industrial Chemistry and performed under scientific supervision of Doctor Rosa Cristina Simões Fernandes, Auxiliary Investigator at the Faculty of Medicine of University of Coimbra and Doctor Mário J. F. Calvete, Assistant Professor, Chemistry Department of University of Coimbra.

November, 2020

Andreia Filipa Nunes de Melo

PHOTODYNAMIC THERAPY WITH GLYCOCONJUGATED PORPHYRINS FOR AGE-RELATED MACULAR DEGENERATION

Dissertation presented to University of Coimbra as a requirement for the degree of MSc in Chemistry, area of specialization in Advanced and Industrial Chemistry and performed under scientific supervision of Doctor Rosa Cristina Simões Fernandes, Auxiliary Investigator at the Faculty of Medicine of University of Coimbra and Doctor Mário J. F. Calvete, Assistant Professor, Chemistry Department of University of Coimbra.

November, 2020

University of Coimbra

Support

This work was conducted at the Coimbra Institute for Clinical and Biomedical Research (iCBR), Faculty of Medicine, University of Coimbra, Portugal in collaboration with the Chemistry Department of University of Coimbra and Centro de Química Estrutural, Departamento de Engenharia Química, Instituto Superior Técnico, Universidade de Lisboa.

The presented work was supported by Programa Operacional Factores de Competitividade COMPETE2020 (CENTRO-01-0145-FEDER-000008: BRAINHEALTH 2020) and by National funds via Portuguese Science and Technology Foundation (FCT): Strategic Projects UID/NEU/04539/2019 (CNC.IBILI), UIDB/04539/2020, UIDP/04539/2020 (CIBB), as well as by COMPETE-FEDER funds (POCI-01-0145-FEDER-007440).

"If we knew what it was we were doing,
it would not be called research, would it?"

Albert Einstein

Agradecimentos

Chega assim ao fim mais uma etapa do meu percurso académico ao fim de 5 anos na Universidade de Coimbra. Este último ano foi o mais desafiador e diferente, mas é com muito orgulho e alegria que chego ao fim desta etapa. Não foi um ano de todo fácil. Foi um ano de muitas mudanças, de descobertas, de reinvenção, mas acima de tudo um ano de muita aprendizagem. No entanto, não seria de todo fácil ou até mesmo impossível chegar aqui sem o apoio de todas as pessoas, que direta ou indiretamente, me acompanharam, ajudaram e incentivaram a continuar e chegar até ao fim. Assim, deixo aqui o meu mais sincero agradecimento a todos aqueles que estiveram lá e, que nunca me irei esquecer.

À minha orientadora, Doutora Rosa Fernandes, obrigado por me ter acolhido no seu laboratório, por me ter dado esta oportunidade, por ter acreditado em mim e depositado a sua confiança em mim desde o primeiro dia. Por todos os ensinamentos e orientação científica, por nunca me deixar desistir, por fazer crescer em mim, ainda mais, toda a curiosidade pelo mundo científico e por toda a liberdade que me deu na execução de todas as tarefas propostas. Obrigado, acima de tudo, pela amizade, pela partilha de todos os bons momentos e por toda a paciência e persistência ao logo do meu trabalho.

Ao meu orientador, Doutor Mário Calvete, obrigado pela oportunidade, pela sua atenção, disponibilidade e ensinamentos para o desenvolver deste projeto e o esclarecimento de qualquer dúvida.

Ao Doutor João Tomé obrigado por me ter acolhido no seu laboratório logo no início deste percurso e é com muita pena minha que face a toda a situação vivida atualmente, que não consegui voltar. Obrigado pela constante disponibilidade, por toda a confiança, incentivo, ensinamentos, oportunidade e pela ajuda para a possível realização deste projeto.

Ao Professor Doutor Carlos Fontes Ribeiro por me ter dado a oportunidade de elaborar o trabalho desta tese de dissertação de mestrado na Faculdade de Medicina da Universidade de Coimbra.

À Sandra e à Sara obrigado por me acolherem no vosso laboratório no início deste projeto, por todo o companheirismo, pela amizade, pela ajuda e disponibilidade dentro e fora do laboratório.

À minha colega de laboratório e, acima de tudo, amiga, Beatriz Martins, não tenho palavras que cheguem para agradecer. Obrigado por acreditares em mim desde o início, nunca me deixares desistir e me mostrares que tudo é possível quando queremos. Por toda a partilha de conhecimentos no laboratório, por nunca te cansares de me ajudar e ensinar e por me ouvires sempre até ao fim em qualquer dúvida e ideias que me surgiam. Obrigado pela amizade e apoio, mas acima de tudo obrigado por estares sempre lá para me apoiar.

Às minhas colegas de laboratório, Madania e Joana, obrigado por todo o companheirismo todos os dias passados no laboratório, pelo apoio e disponibilidade e por todas as conversas tidas dentro e fora do laboratório e, acima de tudo, obrigado pela amizade.

Ao André Alves e ao Pedro, os colegas do laboratório ao lado, obrigado pelas conversas, pelos bons momentos, pela amizade e paciência durante o decorrer deste ano.

À minha afilhada, Patrícia Matos, obrigado por todos os conselhos e paciência, pela amizade e por compreendes sempre que não consegui estar presente durante este ano.
À Soraia Assis obrigado pelo apoio, amizade e ajuda neste ano. Obrigado por veres em mim o que muitos não viram e me fazeres acreditar mais em mim. Obrigado por todas as conversas, mesmo quando não percebias nada do que dizia, pelos conselhos e bons momentos. Obrigado por estares sempre la quando precisava, por me fazeres acreditar que é possível.
À Joana e Ana Maria, que sempre estiveram presentes desde o primeiro dia na universidade. Obrigado pela amizade, pela paciência, por todas as conversas, pelos bons e maus momentos e por, acima de tudo, compreenderam quando estive menos presente e mesmo assim continuarem aqui sempre ao meu lado.
À Rita, Carolina, Pedro, Rui Santos, Rui Frias, Amílcar e João, embora mais distantes, obrigado pela amizade durante o meu percurso na universidade e pela partilha dos bons e maus momentos.
Aos meus amigos Anabela, Adriana, Hugo, Fred, João e Cristiana, obrigada pela amizade e acima de tudo pelos bons momentos partilhados ao logo desta etapa.
Ao André obrigado por toda a paciência, por nunca desistires e nunca me deixares desistir. Obrigado por todo o amor, carinho, amizade, paciência e por compreenderes sempre que chegava mais tarde ou não tinha tempo, por acreditares em mim até ao fim. Obrigado por todos os conselhos, por estares sempre lá mesmo quando achava que mais ninguém estava e por aturares o meu mau feitio sempre que andava nervosa, por não me deixares baixar os braços e fazer acreditar que tudo é possível.
Por fim, a toda a minha família, os mais importantes em todos este percurso, um obrigado por tudo. À minha irmã, Vânia, obrigado por todas as conversas, amizade, ensinamentos. Obrigado por compreenderes quando dizia que não tinha tempo e até mesmo quando me "obrigavas" a sair, por me aturares durante os meses que estivemos em casa e por me ensinares sempre a ver as coisas de uma perspetiva diferente e a não levar tudo tão a sério.
Aos meus pais, Irene e Francisco, obrigado por me ensinarem tanto até hoje, obrigado por fazer o possível e impossível para conseguir tudo o que tenho hoje, por me ajudarem sempre que precisei, por serem o meu apoio em tudo e darem sempre o vosso apoio em todas as etapas e desafios que tive até hoje. Obrigado por me darem esta oportunidade, por todo o carinho e conselhos. Obrigado, acima de tudo, por tornarem tudo isto possível!

À Universidade de Coimbra e, em muito especial, ao Departamento de Química e à Faculdade de Medicina da Universidade de Coimbra, e em especial ao iCBR muito obrigado.

Table of Contents

Abbreviations

$^1O_2$ – Singlet oxygen

^{1}PS – Photosensitizer in the ground-state

^{1}PS* - Photosensitizer in the excited-single-state

$^3O_2$ – Triple-state oxygen

^{3}PS*- Photosensitizer in the excited-triplet state

AGE - Advanced glycation end products

AMD – Age-related macular degeneration

BCA - Bicinchoninic acid

BRB – Blood-retinal barrier

BrMb- Bruch's membrane

CNV – Choroidal neovascularization

DHE – Dihydroethidium

DMSO – Dimethylsulfoxide

EMT- Epithelial-mesenchymal transition

FDA – Food and drug administration

FGF – Fibroblast growth factor

Gal – Galectin

GLUT – Glucose transporter

HP – Hematoporphyrin

HpD – Hematoporphyrin derivative

IR – Infrared

ISC – Intersystem crossing

LEDs- Light-emitting diodes

MTT - 3-[4,5-dimethylthiazol-2-yl]-2,5-diphenyltetrazolium bromide

PBS - Phosphate buffered saline

PDT- Photodynamic Therapy

PS – Photosensitizer

ROS – Reactive oxygen species

RPE - Retinal pigment epithelium

SDS – Sodium dodecyl sulfate

TNF – Tumor necrosis factor

UV – Ultraviolet

VEGF – Vascular endothelial growth factor

α-SMA - α-smooth muscle actin

Abstract

Age-related macular degeneration (AMD) is a retinal degenerative disease that affects the central portion of the retina, called the macula, being responsible for central vision loss. AMD can progress to two advanced stages, dry and wet. Advanced dry AMD is characterized by geographic atrophy of the retinal pigment epithelium (RPE). Wet or neovascular AMD is characterized by choroidal neovascularization (CNV) and, in some cases, RPE detachment occurs and is accompanied by subretinal fibrosis formation. Nowadays, anti-vascular endothelial growth factor (VEGF) therapy has been the first choice for neovascular AMD in order to inhibit CNV. However, in a high proportion of patients with AMD, this therapy is not able to stop the progression of the disease and it has several associated adverse effects. In some cases, photodynamic therapy (PDT) is used in combination with anti-VEGF therapy. The main purpose of PDT is the destruction of the abnormal vessels originated in the choroid that invade the overlying RPE monolayer and neuronal retina. However, to the best of our knowledge, any applied treatment to date can prevent or treat subretinal fibrosis.

The main purpose of this study was to assess the cytotoxicity on ARPE-19 cells (with a mesenchymal spindle-shaped morphology, expressing α-SMA and galectin-1) after PDT with glyco-conjugates (**H_2TPPF$_{16}$(SGlc)$_4$**) and zinc-porphyrin conjugated with four glucose molecules (**ZnTPPF$_{16}$(SGlc)$_4$**). To evaluate the efficacy of the two photosensitizers (PSs), *in vitro* studies were performed to determine the cellular uptake, reactive oxygen species (ROS) production and their toxicity in darkness and after photoactivation.

Both glyco-conjugates were shown uptake by ARPE-19 cells. The presence of sugar-binding proteins in ARPE-19 cells, such as galectin 1, may influence the PSs uptake. The presence of a metal in the porphyrin can also interfere with the uptake. In fact, **ZnTPPF$_{16}$(SGlc)$_4$** showed a slight higher cellular uptake than **H_2TPPF$_{16}$(SGlc)$_4$**. The levels of ROS after PDT were higher in **ZnTPPF$_{16}$(SGlc)$_4$** than in **H_2TPPF$_{16}$(SGlc)$_4$**. Both PSs were non-toxic until activation by light. Both PS demonstrated high efficacy in inducing phototoxicity in ARPE-19 cells.

The obtained results support the idea that PDT with glyco-porphyrins can be a promising therapeutic option to attenuate subretinal fibrosis formation and eventually CNV, which deserves a more detailed study.

Resumo

A degenerescência macular da idade (AMD) é uma doença degenerativa da mácula da retina, e que leva à perda progressiva da visão central em idades mais avançadas. A fase mais avançada da doença pode ser dividida em dois tipos, a forma seca e a forma neovascular. A forma seca é caracterizada pela atrofia geográfica do epitélio pigmentado da retina (RPE), enquanto que a forma neovascular ou húmida é caracterizada por neovascularização coroideia (CNV) e, em alguns casos, pelo descolamento do RPE e fibrose sub-retiniana. Atualmente, a terapêutica de primeira linha da AMD húmida são os fármacos anti-angiogénicos. Injeções intravítreas de anti-VEGF (fator de crescimento endotelial vascular) são indicadas para inibir a proliferação de novos vasos coróide. Em certos casos, contudo, esta abordagem terapêutica com anti-VEGF não é capaz de prevenir a progressão da doença e apresenta muitos efeitos adversos. Em alguns casos, a terapia fotodinâmica (PDT) é usada em combinação com a terapia anti-VEGF. O uso de PDT tem como objetivo a destruição seletiva dos novos vasos anómalos da coróide que podem proliferar e penetrar na membrana de Bruch. No entanto, até ao momento, não existe nenhum tratamento capaz de prevenir ou tratar a fibrose sub-retiniana.

O principal objetivo deste estudo foi avaliar a citotoxicidade induzida por PDT utilizando dois fotossensibilizadores (PSs) glico-conjugados: **H_2TPPF$_{16}$(SGlc)$_4$** e **ZnTPPF$_{16}$(SGlc)$_4$**. Como modelo de estudo utilizou-se a linha celular ARPE-19 (com morfologia mesenquimal fusiforme e expressão de α-SMA e galectina-1). Para avaliar a eficácia dos dois PSs, foram realizados estudos *in vitro* para determinar a sua captação pelas células, a produção de espécies reativas de oxigénio (ROS) e a sua toxicidade no escuro e após fotoativação.

Ambos os glico-conjugados foram captados pelas células ARPE-19. A presença de proteínas com domínios de reconhecimento de carbohidratos e afinidade para galactosídeos, como a galectina-1, e a presença de um metal na estrutura da porfirina podem influenciar a captação destes PSs. Na verdade, o **ZnTPPF$_{16}$(SGlc)$_4$** apresentou uma captação celular ligeiramente superior ao **H_2TPPF$_{16}$(SGlc)$_4$**. Os níveis de ROS após PDT foram superiores com o **ZnTPPF$_{16}$(SGlc)$_4$** do que com o **H_2TPPF$_{16}$(SGlc)$_4$**. Ambos os PSs demonstraram eficácia na indução de fototoxicidade em células ARPE-19.

Os resultados obtidos suportam a ideia de que a PDT com glico-porfirinas pode ser uma abordagem terapêutica promissora para atenuar a formação de fibrose sub-retiniana e, eventualmente CNV, o que requer um estudo mais detalhado.

Chapter I

Introduction

1.1 The eye

The human eye is comprised by several structures with complex functions, including the ability to regulate the amount of light that enters in the eye, to focus on near and far objects or to continuously convert the light into electrical impulses that are carried to the brain along the optic nerve, for image formation. The front part of the eyeball is a transparent structure, called cornea, which occupies approximately one-sixth of it.[1] The remaining part is an opaque structure called sclera. Anatomically, the anterior part of the eye is composed by the cornea, lens, pupil, aqueous humour and iris, and the posterior segment is composed by the vitreous humour, the retina the choroid and, outermost, the sclera **(Figure 1)**.[1, 2]

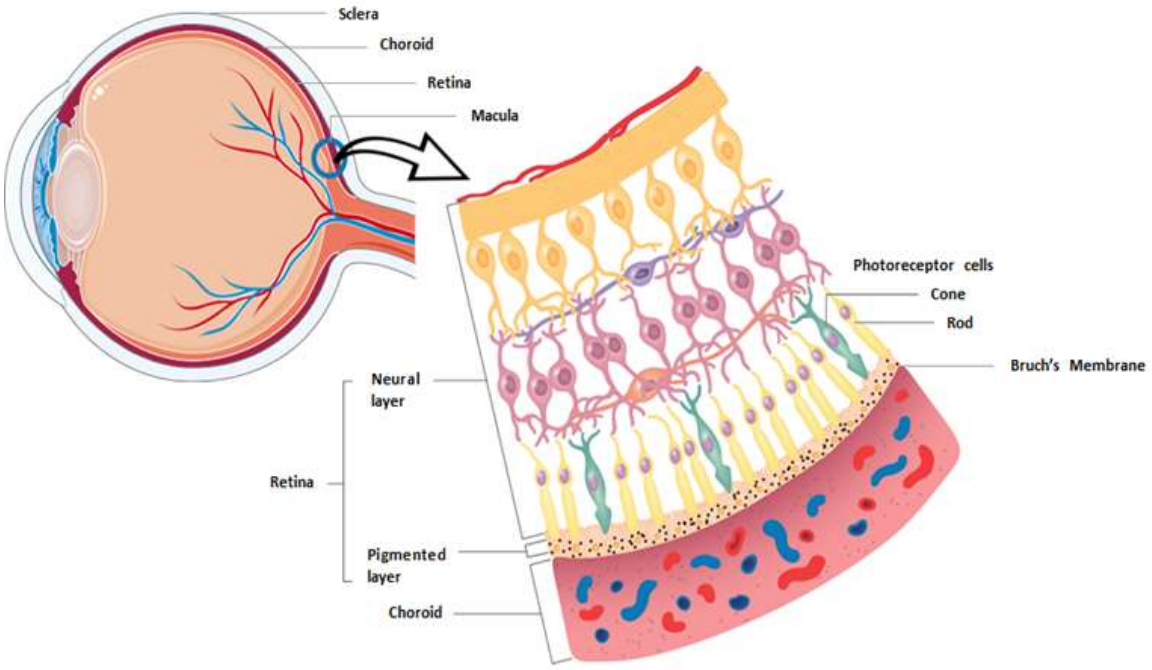

Figure 1. Eye and retina structure. The eye is surrounded by three tissues layers: sclera, choroid and retina. The retina is divided into neural retina, which contains the photoreceptor cells and in the outermost region of the retina, a supportive retinal pigmented epithelium (RPE) layer is present, which is attached to the Bruch's membrane, and is located between the choroid and neural retina. Adapted from: https://smart.servier.com/smart_image/eye/ and https://retinavitreous.com/patientinfo/fundoscopy.php (accessed at October 23, 2020)

The eyeball has three layers or coats: the sclera and the cornea, as the outermost coat; the vascular coat or uveal tract, which constitute the middle layer, comprising the choroid, the ciliary body and the iris; and the retina, as the innermost layer, containing the light-sensing cells (photoreceptors) and the blood vessels that provide nourishment to the inner layers of the retina.[2] Funduscopic examination through an ophthalmoscope allows to illuminate and see the interior of the eye, being crucial in assessing the health of the retina.

1.2 The retina

The retina **(Figure 1)**, a highly specialized neural tissue, is responsible for the conversion of light into electrochemical impulses. It is composed of two layers, the inner neurosensory layer, and the outer pigmented layer composed by retinal pigment epithelium (RPE) cells which are tightly attached to the choroid. The neurosensory layer, also called neuroretina, is essentially made up of neural cells (photoreceptors (cones and rods), ganglion cells, bipolar cells, amacrine cells and horizontal cells), glial cells (Müller cells, astrocytes and microglia), RPE cells and the cells that compose the retinal vessels (endothelial cells and pericytes).[3]

The retina is a high metabolic-rate tissue, needing a constant delivery of oxygen and nutrients which is given by two distinct vascular structures, the intra-retinal vessels and the choriocapillaris. It has two distinct barriers, the inner and the outer blood-retinal barrier (BRB). Both contribute to the maintenance of retinal homeostasis through the regulation of the flux of nutrients, ions, water, metabolites and even harmful toxins between circulating blood and the retina. Besides this, the integrity of the BRB is crucial to prevent the exposure of the neural tissue to circulatory factors such as antibodies and immune cells. The inner BRB is formed by retinal microvascular endothelial cells. However, other retinal cells, such as pericytes and retinal glia (Müller cells and astrocytes) are important in the development and maintenance of the integrity of this barrier.[4] The outer BRB is formed by the RPE cells that restrict the passage of fluid and molecules between the choroid and the subretinal space. Complex and dynamic structures called tight junctions are key components of the two retinal barriers.[4]

The two types of photoreceptors, rods and cones, in the neuroretina, are specialized neurons responsible for the phototransduction. This process consists of converting light into signals that will stimulate the transmission of neuronal impulses, leading to changes in the cell membrane potential after absorption of a photon. Posteriorly, these signs are transmitted to the brain through the optic nerve where they are converted into vision.[5] Underneath photoreceptors is the layer of pigmented cells, the RPE. This layer is formed by a single layer of hexagonal, polarized and pigmented cells which have several functions such as absorption of the excess of light that enters the eye and is not absorbed by the photoreceptors, formation of the outer BRB and phagocytosis of the outer segments of photoreceptors.[5, 6] Between the RPE and the choroid is a thin membrane called Bruch's Membrane (BrMb). It is composed by the RPE basement membrane, an inner and outer collagenous layer, a central elastic layer and the choriocapillaris endothelium basement membrane. This thin and semipermeable membrane gives support to the RPE monolayer and, as previously mentioned, controls the transfer of biomolecules, creating a biochemical and physical barrier between the retina and the choroid.[7,8] The choroid is a vascular layer that supplies oxygen and nutrients to the RPE and outer retina and also contributes to the maintenance of the temperature and volume of the eye. Morphologically, it can be divided into four layers: choriocapillaris, near to BrMb, a medium-sized vessel and tapetum layers, large-vessel layer, and suprachoroidea. The vessels in choriocapillaris are fenestrated and external to their endothelium.[5, 8]

1.3 Age-Related Macular Degeneration

AMD is a degenerative disorder that affects the central part of the retina, the macula. This pathology affects essentially people over 50 years old being the leading cause of central vision loss in the elderly. AMD is characterized by a progressive loss of visual function due to progressive degeneration of the macula, as a result of abnormalities of photoreceptors, RPE, BrMb, and the choroid, which can lead to irreversible central vision loss.[5, 9] The macula comprises only 4% of the entire retinal area, but represents almost 10% of the entire visual field. This area is responsible for all the central vision, the colorful vision, and is responsible for seeing fine details.[10] Therefore, lesions that develop in this region can have serious consequences on visual function. The clinical classification of this pathology is divided into three stages: early, intermediate and late AMD. The advanced stage can be classified into two types: atrophic or dry AMD and neovascular or wet AMD, depending on the lesions (**Figure 2**).

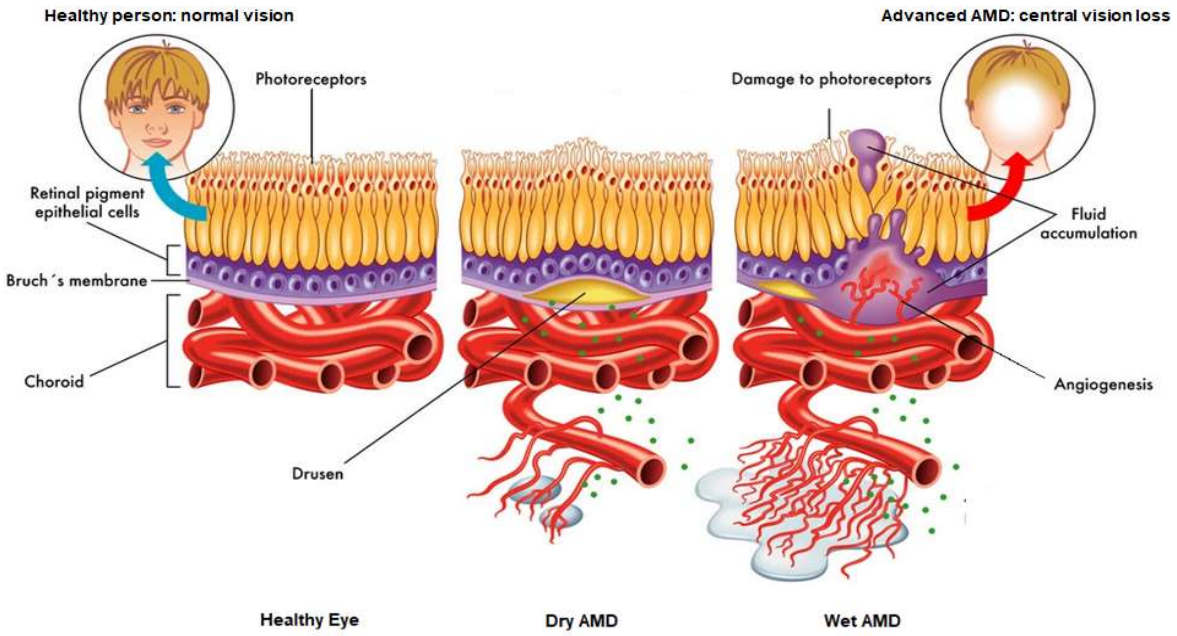

Figure 2. Schematic of retina and choroid: (A) healthy eye with intact retina and choroid; (B) dry AMD with the presence of drusen between RPE layer and BrMb; (C) wet AMD with formation of abnormal new blood vessels (angiogenesis) in choroid, subretinal hemorrhage, fluid accumulation and, consequently, visual impairment. Adapted from [21]

Besides the above-mentioned functions of the RPE, it plays a pivotal role in eliminating the waste from photoreceptors, by degrading or recycling it and exocytosing some material for removal by the choriocapillaris. However with age, RPE can become dysfunctional which can cause an accumulation of these components between the RPE and the underlying basement membrane, the BrMb, which can both lead to the formation of yellow deposits underneath RPE layer called drusen and increased permeability of the RPE layer. [5]

"Normal" drusen, that commonly appear with age, are small with a size of ≤ 63 μm. Small drusen are inoffensive and, usually, are not associated with any vision problems. Early AMD is diagnosed when there is

an abnormal accumulation of drusen that have a size between >63 μm to ≤125 μm, called medium-sized drusen. Usually, this stage is not characterized by pigmentary abnormalities. In fact, this stage is asymptomatic which is the reason why, in most cases, AMD is only diagnosed in a most advanced stage. Early AMD can develop to the intermediate stage, which is characterized by large drusen, with size >125 μm, associated with pigmentary abnormalities in the macula. Pigmentary alterations can be defined as hyper- or hypopigmentation. In this stage, some patients suffer from a blurred spot in the center of their vision which cause them the need to increase light to read and perform other tasks that require detailed vision. [11, 12] Besides that, there is another classification for drusen type: hard drusen, which are small drusen (≤63 μm), discrete yellow-white spots that are commonly identified in many populations and do not present risk of vision loss; and soft drusen, which have a medium-size or greater (≥ 63 μm) and are associated with a higher risk for the development of advanced AMD, especially neovascular AMD. [9] In early AMD, the presence of drusen are not associated with vision loss. However, in more advanced stages of AMD, drusen formation and consequent accumulation over time leads to RPE dysfunction, which can cause photoreceptors death and consequent vision loss.[13]

1.3.1 Prevalence, incidence and risk factors of AMD

According to the World Health Organization, blindness and vision impairment affect at least 2.2 billion people worldwide and 1 billion have sight loss that could have been prevented or treated.[14] Globally, AMD is the third main cause of blindness after cataracts and glaucoma, but in industrialized countries is the primary cause in the elderly. In a meta-analysis made in 2017, the global prevalence of any type of AMD has been reported to be 8.7%, but the prevalence rate of European population is higher compared to the global estimate.[15,16] In fact, in Europe the majority of blindness and severe vision loss is due to AMD. In 2017, was estimated that 34 million Europeans over the age of 60 are affected by any type of AMD, which 2.8 million have any advanced form of AMD and 1.7 million of these have the wet form of the disease. Being this disease a serious health problem, and according to the increase of the average life expectancy of European population it is expected a 20-25% increase until 2050.[17, 14]

Until today, the exact mechanism involved in the onset of AMD remains unknown and the multifactorial nature of AMD, the complexity of the visual system, and the enigma of aging processes make this pathology very complex. However, it is known that the combination of demographic, environmental, and genetic factors are involved in AMD progression.[18, 19]

Age is the most important risk for the development and progression of AMD. A recent analysis of AMD prevalence in Europe, combining data of 14 population-based studies including Portugal, reveals that the prevalence of early AMD increases from 3.5% to 17.6% from the age of 55-59 to the age of ≥85 years old and for late AMD those numbers are 0.1% and 9.8%, respectively. [20]

Additionally, cigarette smoking, ultraviolet (UV) exposure, diet, and physical activity are other important environmental risk factors. [21] In fact, one study revealed that current smokers younger than 85 years had a 6.6-

fold increased risk of neovascular AMD versus those who had never smoked. Moreover, former smokers had a 3.2-fold increased risk of it and after 20 years cessation of smoking, the risk decreases to the same of the non-smoker patients.[22]

The continued exposure of retina to light throughout life can lead to retinal damage, namely long-term sunlight exposure. Visual perception results from a response when visible light (400 - 760 nm) radiation reaches the retina. Visible light is between infrared (IR) radiation (>760 nm) and UV light (<400 nm). Until 295 nm the UV light is absorbed and blocked by the cornea and lens, however, some UV light reaches the RPE. With continuous light exposure, mainly UV light, the retina becomes highly susceptible to photochemical damage. Usually, there is a protective mechanism of the retina against light damage. However, with age there are structural and functional changes in the retina, which predispose the development of AMD. Notwithstanding, continued light exposure is one of the main risk factors for the onset and progression of AMD. [18, 23]

A diet rich in antioxidants with high consumption of fruits, vegetables, legumes, grains, moderate consumption of fish, and limited red meat is associated with a decreased risk of AMD. However, elevated consumption of carbohydrates increases the risk of developing the disease. Nevertheless, regular exercise is associated with an increase of antioxidant enzymes activity, which consequently a decreases the risk of AMD.[18] Oxidative stress, mainly induced by reactive oxygen species (ROS) generated by the oxygen-rich environment and the exposure to light in the eye, is believed to contribute to the development of AMD, mainly, in generating cellular damage in RPE cells. In normal conditions, the amount of ROS is counterbalanced by cellular antioxidants mechanisms, where antioxidants enzymes are present. Antioxidant enzymes play an important role against ROS and changes of their expression or/and activity seems to be associated with AMD development.[24] Based on this, diet rich in antioxidants and/or the increase of antioxidant enzymes activity in regular exercise will help in cellular antioxidants mechanisms.

Besides the environmental and demographic factors, genetic factors and the presence of some comorbidities are also involved in the development of AMD. A Genome-Wide Association Study in 2016 has identified common and rare genetic variants in 34 genetic loci, which are involved in the complement system, extracellular matrix remodeling, and lipid metabolism, and appear to play an important role in the development of AMD.[18,25] For example, some studies have been reported the involvement of common variants of the complement factor H gene in AMD onset and progression. Also, genes encoding proteins of the lipid metabolism are also involved in drusen formation, contributing to AMD development. Besides that, the presence of some other comorbidities such as cataracts, hypertension, diabetes or Parkinson's disease, may contribute to AMD development.[18]

Although dry and wet AMD, the two forms of the advanced stage of the disease are characterized by the presence of drusen and pigmentary alterations, their main features are geographic atrophy and neovascularization, respectively. [10, 11, 13]

The precise mechanisms underlying both forms of advanced AMD are not yet fully understood. In some cases, patients develop neovascular AMD after developing atrophic AMD which could indicate that neovascular AMD is a most progressive form then atrophic AMD.[13, 26] However, there are some occasional patients without

any prior sign of atrophic AMD that show neovascular or exudative changes as the first manifestation of the condition, being these patients diagnosed with neovascular AMD without previous development of dry AMD.[10]

1.3.2 Dry AMD

Comprising 80-90% of all diagnosed cases, atrophic AMD represents the most common type.[13] Besides the presence of drusen, the atrophic form is characterized by the appearance of geographic atrophy in the RPE. The geographic atrophy of RPE can be detected by sharply demarcated by hypo- and depigmentation of RPE, where the RPE layer becomes thin and allows the visualization of underlying choroidal vessels in the eye examination. Although the exact mechanism underlying the development of geographic atrophy is not completely understood, it is known that this atrophy was not limited to RPE only, but also involves photoreceptors dysfunction and degeneration as well as choriocapillaris loss.[27] Usually, dry AMD has a slow progression, with a gradual loss of visual function during several years. Many patients with this form are asymptomatic and, because of this, unaware of the disease. Although, in some patients (10-15%) the progression can be more rapid and serious, causing significant vision loss due to geographic atrophy.[10]

1.3.3 Wet AMD

Neovascular AMD represents a small proportion of AMD cases, it is the more severe and dangerous form, being associated with severe vision loss.[28] This form of the disease is characterized by choroidal neovascularization (CNV) and, in some cases, RPE detachment and, consequently, subretinal fibrosis.[29]
The process of new blood-vessel growth from the existing vasculature is called angiogenesis.[30] The term of angiogenesis is normally associated with tumors formation but also occurs in a range of non-neoplastic diseases like diabetic retinopathy and neovascular AMD. Usually, this process is regulated by a balance between pro- and anti-angiogenic factors. However, this balance can become dysregulated under certain circumstances, such as ischemia, hypoxia, or inflammation.[31] Ocular angiogenesis affects almost all tissues of the eye and the choroid is no exception.[32] CNV is the formation of pathological blood vessels in the choroid that will cross trough BrMb and RPE, resulting in the accumulation of intraretinal and subretinal fluid and detachment of the photoreceptors from the RPE.[10, 9, 32] CNV, in end-stage of the disease, results in a fibrovascular or atrophic macular scar, and permanent loss of the central vision which, in more serious cases, can cause total vision loss.

1.4 Galectins and wet AMD

Galectins (Gal) belong to a family of animal lectins and, to date, 15 Gals have been identified.[33] These lectins are characterized by affinity to β-galactosides and the presence of at least one evolutionary conserved

carbohydrate-binding domain.[34, 35] The Gal family can be divided in three groups, based on their structure and number of carbohydrate recognition domains: homodimers, which contain a single carbohydrate recognition domains and include Gal-1, -2, -5, -7, -10, -11, -13, -14, -15; Gals with tandem-repeats, which include Gal-4, -6, -8, -9, -12, containing double and non-identical carbohydrate recognition domains; and the chimera subfamily, which include Gal-3, and contains one carbohydrate recognition domain connected to a non-lectin domain and is capable of forming a multimeric structure.[33] Gals can be found in the nucleus, cytoplasm, cell surface, extracellular matrix, and biological fluids.[35]

Several studies suggest that members of the galectin family play a critical role in angiogenesis.[32, 33] In terms of ocular angiogenesis some studies suggest that Gal-1 and Gal-3 play a key role in the angiogenic process, and, beyond angiogenesis, Gal-1 are also involved in subretinal fibrosis.[32,36] Gal-1 is described as being involved in vascular endothelial growth factor (VEGF)-receptor segregation, internalization, and trafficking, endothelial cell proliferation, migration and morphogenesis, vascular permeability, and angiogenesis. Besides that, Gal-1 is suggested to be associated with the angiogenic process in cancer and diabetic retinopathy.[37, 38] One recent study refers the influence of Gal-1 in CNV in patients with neovascular AMD.[36] This study revealed that overexpression of LGALS1, the gene that encodes Gal-1, increases the CNV, and these AMD patients showed a co-localization of Gal-1 with VEGF-receptor in neovascular endothelial cells which suggests Gal-1 as a key CNV promoter in AMD patients. Moreover, this study revealed that Gal-1 was also involved in subretinal fibrosis, that also occurs in neovascular AMD. [36]

Gal-3 plays important roles depending on the cell site: intracellularly, it protects cells against apoptosis through a carbohydrate-independent mechanism; extracellularly, it mediates cell-cell and cell-matrix interaction.[35] Over the years, some reports have shown that Gal-3 has a role in disease processes, including in ocular diseases. Some studies have found a correlation between Gal-3 and some angiogenic factors. [32, 35, 39] For example, Gal-3 plays an important role in VEGF- and bFGF-mediated angiogenic response which suggests that Gal-3 can be implicated in pathologies like diabetic retinopathy and wet AMD.[32, 35] Besides this, it has been reported co-localization of Gal-3 with VEGF-receptor in neovascular eye tissue which suggests the involvement of Gal-3 in CNV.[35] Other interesting research is about the correlation between Gal-3 and advanced-glycation end products (AGEs), which are also known to play an important role in the induction of CNV. It has been reported the accumulation of these products in RPE and BrMb, as well as, their presence in drusen constitution.[5] Gal-3 levels have been found to be increased in dry AMD. This protein has been described as an AGE receptor.[40] These results have shown the possible role of the AGEs and Gal-3 in the progression of dry AMD to wet AMD.

1.5 Treatments for AMD

Although until today there is no cure for AMD, there are some therapies available to prevent or slow down the progression of the disease. In early dry AMD, the treatment used is generally nutritional therapy and control of

modifiable risk factors such as smoking, hypertension, and body-mass index.[41, 42] Some studies related to age-related eye diseases have been shown that using antioxidant, multivitamins and zinc in patients with early dry AMD can be effective in reducing the risk of developing advanced AMD and associated visual loss.[43, 44]
In advanced and serious AMD stages, especially in neovascular AMD, there are various treatment options available, being the most commonly used the laser photocoagulation, anti-VEGF injections and photodynamic therapy (PDT), which will be forth discussed.

1.5.1 Laser Photocoagulation

Laser photocoagulation was the first treatment used in the management of neovascular AMD. This therapeutic approach uses an intense beam of light or laser to burn small areas of the retina, corresponding to areas of fragile and leaky blood vessels in the retina. This approach allows for abnormal blood vessels sealing, slowing their leakage and consequently reduces central vision loss. However, in some cases, the procedure of laser burns in the retina can be associated to some additional vision loss, *i.e.,* a blind spot where the laser creates a scar. Moreover, in some cases, the vision loss during the treatment can also be worse than vision loss if this treatment is not preformed. Furthermore, this procedure can cause eye bleeding, retinal damage and the growth of more abnormal blood vessels. With the appearance of new therapeutic approaches over the last decade, laser photocoagulation is only used in a small proportion of patients with wet AMD.[42, 45]

1.5.2 Anti-Vascular Endothelial Growth Factor

CNV was defined as the growth of abnormal blood vessels underneath the retina, in the choroid, and this process begins when the endothelial cells of a mature blood vessel wall begin to proliferate due to the presence of angiogenic factors, but the exact molecular mechanism remains unclear.[46] It is known that this phenomenon is stimulated by angiogenic factors like VEGF, insulin-like growth factors, fibroblast growth factor (FGF) family members, and angiopoietins.[5,46] VEGF seems to be the main angiogenic factor in ocular angiogenesis. The sub-family of VEGF includes five members (VEGF-A, -B, -C, and -D and placental growth factor) being VEGF-A the most important factor in neovascularization.[31] RPE, photoreceptors, and endothelial cells play an important role in VEGF production and its levels significantly increase in patients with neovascular AMD.
Nowadays, anti-VEGF therapy is the most commonly treatment used in patients with neovascular AMD since this therapeutic approach has been shown to be quite effective. The main objective of the use of the anti-VEGF-based drugs is the binding and inhibition of VEGF, which lead to the regression of abnormal blood vessels and, consequently, offer a significant vision improvement.[47, 48] However, this therapeutic approach to manage wet AMD is not enough for a total remission of neovascularization, since other factors also seem to play an important role in CNV.

The first anti-VEGF drug approved by Food and Drug Administration (FDA) for the treatment of patients with neovascular AMD (end of 2004) was pegaptanib (Macugen, Pfizer), a small oligonucleic acid molecule. This pegylated oligonucleotide is capable of binding and inhibiting the extracellular isoform of VEGF that are at least 165 amino acids in length (VEGF-165), interrupting the CNV process. However, pegaptanib showed only visual stabilization, without visual gain.[42, 48, 49] In 2007, the FDA approved another anti-VEGF drug, ranibizumab (Lucentis, Genentech, Novartis), which is a humanized antibody fragment, with the ability of binding and neutralizing all the biological active forms of VEGF. [48] This drug was the first treatment that, beyond visual stabilization, also offered substantial visual gain.[47, 50]

Bevacizumab (Avastin, Genentech) is another anti-VEGF drug, approved in 2004 by the FDA as a chemotherapeutic agent for the treatment of colorectal cancer and other neoplastic diseases.[51, 52] This drug is a humanized monoclonal antibody against VEGF, and its activity is similar to ranibizumab. However, bevacizumab is less expensive, yet showing similar efficacy for the management of CNV. Later, in 2005, some further results showed the efficacy of bevacizumab on preventing CNV and, since then, this anti-VEGF is used as a treatment for the wet form of AMD.[52] Besides these anti-VEGF drugs that are monoclonal antibodies, there are also other two VEGF inhibitors, the aflibercept (formerly known as VEGF Trap Eye) and the conbercept, that belong to a different class of drugs, the fusion proteins, which are already used for the treatment of neovascular AMD.[42, 51, 53, 54, 55] The former is a soluble fusion protein of VEGF receptors 1 (Flt-1) and 2 (KDR) to the constant region (Fc) of human immunoglobulin gamma (IgC1) and the latter is also a recombinant fusion protein made of the second Ig domain of VEGF receptor 1 and the third and fourth domains of VEGF receptor 2 to the Fc of human IgC1. The presence of the additional domain 4 of VEGF receptor 2 in conbercept has shown to provide an affinity 50-fold higher for VEGF compared to becacizumab.[56] More recently, in 2019, brolucizumab (Novartis), another anti-VEGF, was approved by FDA. Also known as "KH902", it is a humanized, single-chain variable fragment antibody that inhibits VEGF-A.[57]

Considering all the above, anti-VEGF is the most used and most promising therapy used in the context of neovascular AMD. Until today, encouraging results were obtained using anti-VEGF therapy, which allowed to increase the quality of life of millions of patients suffering from this debilitating ocular disease. However, this therapy not only has some disadvantages that need to be fixed but also there is a significant proportion of patients that do not respond to it. Normally, the anti-VEGF drug is administered through an intravitreal injection and many patients require injections every 4 to 8 weeks.[58] However, these injections are not only uncomfortable, painful and expensive for the patients, but also repeated and long-term injections increase the probability of ocular and systemic complications.[59] Moreover, some studies have been reported that decreased levels of circulating VEGF due to prolonged VEGF inhibition are associated with increased risk of stroke, myocardial infarction and thromboembolic events. Besides this intravitreal administration being used in small doses in order to decrease the risk of these systemic vascular events, it is possible to find, in some cases, levels of VEGF inhibitors in peripheral blood with a concentration above its IC_{50}, which concern the professionals.[42, 60] Other studies showed that an increased use of anti-VEGF therapy in patients with neovascular AMD is associated with an increase in the incidence of RPE tears, which consists of a disruption of the RPE monolayer

and, consequently, development of subretinal fibrosis.[59, 29] In addition to these side effects, inflammation and intraocular pressure elevation, retinal detachment and ocular hemorrhage are other side effects associated to the use of anti-VEGF therapy in neovascular AMD.[59] On the other hand, patients can also develop mechanisms of resistance to anti-VEGF therapy, which leads to a reduction of therapeutic effect in reducing CNV.[61]
Being that, anti-VEGF therapy is intended as the best therapeutic approach to stabilize and improve the visual acuity, but since all about this pathology still remains unclear, this therapy is not enough to cure AMD and the suddenly suspension of its use leads to effectiveness loss. Based on this, it would be necessary to develop new studies to increase the knowledge of this pathology and also develop new therapeutic approaches.

1.6 Photodynamic Therapy

Photodynamic therapy (PDT) is a treatment based on the combination of three components: photosensitizer (PS), visible light, with a specific wavelength, and molecular oxygen.[62, 63] The PDT protocol consists in the administration of a PS to the patient, followed by a waiting period for PS to preferentially accumulate in the target cells. Then, the irradiation of the diseased tissue with light with a specific wavelength results in cytotoxicity induced by reactive oxygen species (ROS) production, which will lead to cell death.

1.6.1 Brief History

The idea of using light as therapy in human diseases has a very long history. Old Egyptian, Chinese, and Indian civilization used the light for the treatment of vitiligo, psoriasis, skin cancer, and even psychosis.[64] The first treatment using sunlight with medical purposes was for skin diseases, around 1400, and recognized as phototherapy.[65] Since then, light as a therapeutic approach has been increasingly used in several pathologies.
Phototherapy can be used with or without PS (a molecule capable of absorbing light energy and transferring this energy to adjacent molecules) using UV or visible light. Without PS, phototherapy is used in dermatology to treat vitamin D deficiency, neonatal jaundice, psoriasis, eczema, and cutaneous T-cell lymphoma. On the other hand, PDT is a type of phototherapy that requires the presence of PS which appeared in the early 1900s, being its clinical use only approved in the 1990s.[65]
At the beginning of the 1900s, in Munique, Oscar Raab and his professor Herman von Tappeiner shown that certain dyes, when exposed to sunlight, can induce cell death in some microorganisms.[66] In 1903, they described the first application of PDT in cancer treatment, when eosin and light were combined to treat skin cancer. [67]
Over the following year, a lot of research was performed to find chemicals that, using light, could induce phototoxicity. In 1911, Hausman performed experiments with Hematoporphyrin (HP) which contributed to a continued interest in research for porphyrin-based PS.[67] A few years later, Schwartz and Lipson found other chemical species denominated Hematoporphyrin Derivative (HpD). This PS demonstrated to be effective in the detection of malignant tissues by the resulting tumor fluorescence in patients.[68, 69] Furthermore, in 1975,

Dougherty, demonstrated that HpD was an effective photosensiting agent in mammary carcinoma, among other types of cancer.[70] In 1993, a purified HpD compound, named Photofrin® was approved for PDT in patients with early and advanced-stage cancer of the lung, digestive, and bladder in Canada, Netherlands, France, Germany, Japan, and United States.[71] Since then, the research for the discover of new and better PSs for different pathologies never stopped. The use of PDT in ophthalmology only appeared in the 1990s. In the AMD context, there is only one PS approved, verteporfin, and is used for the treatment of CNV associated with neovascular AMD.[72]

1.6.2 PDT components

1.6.2.1 Photosensitizers (PS)

Since the first approved PS in 1993, a great effort has been put towards the development of improved and more specific photosensitizing agents. A large number of PS have been developed and tested *in vitro* and *in vivo* for PDT, but only a small number has been proved as nearly ideal or effective. PSs are natural substances or synthetic derivates, ideally without any therapeutic activity until the presence of irradiation. When they absorb light with a specific wavelength, then photophysical and photochemical reactions occur.[73, 74] But what is need for a PS to be "ideal"? Like other types of drugs, an "ideal" PS has a set of distinguished characteristics: a) known chemical composition and stability at room temperature; b) no or minimal cytotoxicity in the dark and cytotoxicity only after irradiation; c) high target selectivity; d) photostability and solubility in aqueous media; e) high molar absorption coefficient in the 600-900 nm range of the electromagnetic spectrum. [62, 74]

The most commonly applied PSs structures in PDT are tetrapyrrolic macrocycle-based compounds, such as porphyrins, chlorins, bacteriochlorins, phthalocyanines, and related structures (**Figure 3**). These structures can be classified into first, second, and third-generation PSs, according to their chemical and biological characteristics. They have a great capacity of conjugation and absorption of visible light, making them colored compounds. [62, 65]

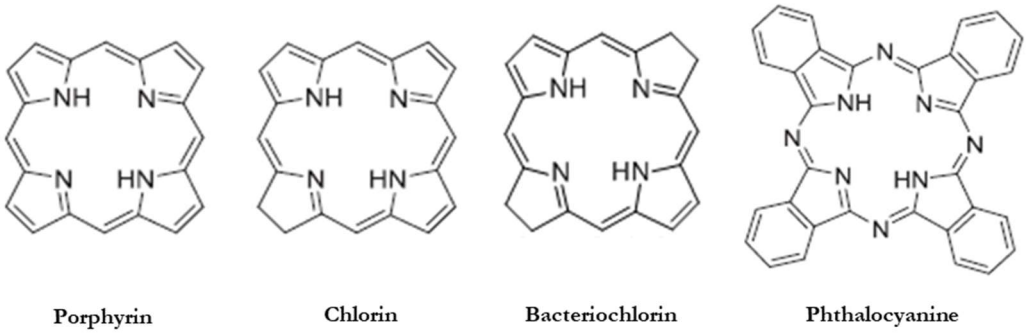

Figure 3. Basic chemical structures of the porphyrin, chlorin, bacteriochlorin and phthalocyanine.

First-generation PS

As previously mentioned, the first approved porphyrin-based PS was photofrin (a HpD), being considered a first-generation PS.[65] This PS was related to the porphyrin structure, which is a structure composed by four modified pyrrole subunits, interconnected by methane bridges (Figure 3). Usually, porphyrins have an absorption spectrum characterized by five peaks between 400 and 600 nm, being the strongest one around 400 nm and known as the Soret or B band, and the other four weaker absorption peaks known as Q-bands. [62, 75] However, these PSs have low solubility and low selectivity to the target and exhibited prolonged photosensitivity and lacked wavelength absorption in the red region of the electromagnetic spectrum, which is the desired window of absorption, where tissues absorb less [65, 76, 77]

Second-generation PS

Porphyrin-related members of PS within second-generation PSs are usually activated at wavelengths in the red and near-IR region, above 650 nm until 800 nm of the electromagnetic spectrum, which is an advantage to tissue light penetration. [65, 78] The most famous members of this sub-family relate to chlorin (Figure 3), the reduced macrocycle of the porphyrin family, including derivatives from chlorophyll or chlorin derivative monoacid ring A, verteporfin (Visudyne ®, Novartis AG, Basel, Switzerland). When compared to porphyrins, chlorins have one of the pyrrole subunits reduced, which makes the intensity of the lowest energy absorption band increase to 640-700 nm.[65, 77]

Also considered as second-generation PSs, phthalocyanines have also emerged as PSs for PDT. Their structure consists of a ring with four isoindole units linked by imine nitrogen atoms. The pyrrole groups in phthalocyanines are conjugated with benzene rings and these compounds require complexation of a metal in its cavity, to exhibit PDT properties, since the presence of transition metals allows the intersystem crossing (ISC). [65, 76] Taking into account their chemical structure, the maximum wavelength can be found at around 670 nm, in the red region of the electromagnetic spectrum. Besides their maximum wavelength in the red region, the second-generation PSs have a higher chemical purity and higher yield singlet oxygen formation. Furthermore, they have a higher clearance which decreases photosensitivity. However, in the case of phthalocyanines, their extended π-conjugation reduces their solubility, which is a limiting factor to their use is biological context. [76]

Third-generation PS

First and second-generation PSs are known for their considerable hydrophobicity and low selectivity. The hydrophobic properties lead to the formation of aggregates in aqueous medium, decreasing the photodynamic effect as well as the selectivity. [79] Over the years, to solve these problems, researchers have developed the third-generation PSs. Being chemically modified, this new generation of compounds presents an improvement in

their solubility and target selectivity. The bioconjugation of PSs, like porphyrin or phthalocyanine derivatives, can be performed using many biocompatible motifs such as monoclonal antibodies, amino acids, carbohydrates, peptides, polyethylene glycol or sugar molecules. [79, 80] Furthermore, other systems for PS delivery were also developed, such as polymer-PS conjugates, liposomes, or polymeric micelles, in order to increase their solubility and selectivity to the target. [80] These types of PSs are a huge advance in science, mainly in PDT research, since they allow to increase at the same time the photodynamic effect and the safety of this therapeutic approach.

Glycoconjugated PS

Over the years, the interest in the third generation PSs has been increased, especially with their conjugation with carbohydrates, such as galactose and glucose.[81, 82] Carbohydrates are involved in many biological processes and they can interact with glycoprotein-based membrane receptors that have carbohydrates recognition domains. Lectins, such as Gals, have carbohydrate recognition domains and, over the years their study for use as a target to drugs have been increasing and help in drug discovery.[82] Based on this, the conjugation of galactose or glucose with PSs has been revealed as an interesting approach in the field of cancer since it allows to increase the local concentration of PSs in tumors tissues where there is an overexpression of some lectins and glucose transporters (GLUT).[83, 84] During the last years, our group has been shown that the use of this type of PS is a promising strategy for PDT in cancer. In fact, we have shown a high uptake and phototoxicity of a galacto-conjugated phthalocyanine in bladder cancer cells, which present high levels of Gal-1 and GLUT1 protein levels.[62, 82]

To date, in ophthalmology field, especially AMD, there are no studies reporting the use of galactose- or glucose-conjugated PSs. Though, it should be interesting to study this PSs in this area, once some studies, as previously discussed, have highlighted the involvement of lectins in the wet form of AMD.

1.6.2.2 Light sources and delivery

The light source and delivery systems are important components of PDT. While the light is essential to activate the PS and promote photodynamic effect, its deliver to the target tissue, using for instance an optical fiber, may promote a selective treatment, sparing the surrounding healthy tissues (which are not irradiated). Lasers and non-laser sources/lamps are some examples of light sources employed in PDT. Lasers can offer a monochromatic and powerful source of light that can reduce the time necessary to deliver the appropriate amount of light to the tissue. Since lasers emit monochromatic light, it is necessary to choose the laser wavelength to match with the absorption band of the PS. Argon lasers and argon-pumped dye laser, metal vapor-pumped dye laser and diode laser are some examples of lasers used in this therapy. With light delivery devices, such as optical fibers, it is possible to perform a direct irradiation into the lesions located in inaccessible sites. [85, 86]

Lamps are the first light source used in PDT and they offer a broad range of wavelengths. However, it is necessary an appropriate optical filtering to ensure unnecessary wavelengths and to match to the photoactivation PS wavelength. This type of light source cannot be used in small optical fibers (poor beam quality, large beam size, and small density) in order to limit their use to skin/superficial lesions. Fluorescence, incandescent, metal halide, xenon arc, and sodium arc lamps are other lamp sources that can be used in PDT. In general, lasers are more expensive than lamps, but lamps are easier to use (more friendly) and useful to treat large superficial lesions.[85, 86]

Over the years, other sources of light have been developed: light-emitting diodes (LEDs) and femtosecond solid-state lasers. LEDs are less expensive and offer advantages not only for clinical use. Normally, LEDs are small, portable, adaptable and, similar to lasers, can be used for endoscopic or interstitial applications, in superficial tumors. In LED devices, it is possible to choose emission wavelength ranges from 350 nm to near 1100 nm. However, this source has some concerns, such as thermal effects, especially when used in interstitial PDT. Femtosecond solid state lasers are described as a two-photon PDT since it results from two-photon excitation. This phenomenon is based on the incidence of light that is characterized by a higher photon density. The PS can absorb two photons of equal energy simultaneously, exciting an electron to an energy level that is equal to the sum of the energy of two absorbed photons. For example, porphyrins are excited in the 400-500 nm region, however, using this light it could be excited in the 800 – 900 nm region. This feature is very important since it allows a higher penetration into the tissue, which would increase the depth of PDT. However, this type of lasers is difficult to maintain and to operate, requiring additional specialized professionals.[85]

The choice of light source for PDT depends not only on the PS and their absorption properties, but also on the light dose and on the location and optical characteristics of the target tissues.[62] The light source must be able to activate the PS with an appropriate wavelength and dose and to cross the human tissues until the target. Normally, PSs are activated with light in the region of visible light. Light penetration depth into a tissue increases with the wavelength. Blue light has a weak penetration capacity compared to red light, which has a penetration capacity around 4-5 mm, which is interesting for PDT. However, the optical characteristics of tissues are also important, since light penetration reduces in optically dense tissues. The use of delivery devices, such as optic fibers, can increase the efficacy of light delivery and increase the penetration of light into the tissues to activate some PSs in several diseases. In ophthalmology, such in AMD context, the choice of type of light and light sources is crucial. Light exposure, mainly UV light, are involved in AMD progression, once their continued exposure can lead to retina damage.[87]

1.6.3 Photophysics and photochemistry

The main photophysical processes and photochemical reactions of PDT are represented by the Jablonski diagram (Figure 4). Usually, PSs are in the lowest energy level, named ground-state (^{1}PS). This normal state, ^{1}PS, is characterized by a paired electron with opposite spins. After the absorption of light, with a specific wavelength, a transformation of the PS to the excited-singlet-state (^{1}PS*) will occur. This means that one of the two electrons of ^{1}PS is removed to an empty higher-energy orbital. The excited-single-state is very unstable with a half-life generally less than 1 μs. [62] In this state, the PS can return to the ground state by emitting a fluorescent photon or may undergo to a process called ISC ascending to a excited-triplet-state (^{3}PS*) with two electrons unpaired with parallel spin. This new state has a longer half-life time than ^{1}PS* and can return to the ground state by emitting phosphorescence or transferring the energy to another molecule. When the PS restores to its ground-state the cycle is repeated.[76, 88, 89] Although, depending on the conditions, two types of photochemical reactions can occur to induce photodynamic effect: Type I and/or Type II reactions. It is assumed that type I reaction becomes more dominant under hypoxic conditions and type II reaction is pinpointed as the most important photochemical reaction associated to the photodynamic effect.[74, 76]

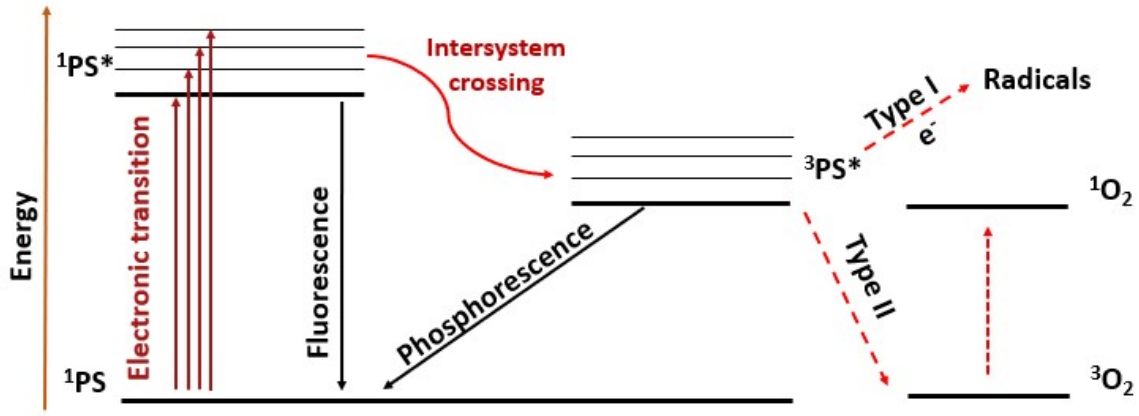

Figure 4. Jablonski diagram showing the excitation of photosensitizer (PS) and type I and II photochemical reaction in photodynamic therapy (PDT).

1.6.3.1 Type I photochemical reaction

Usually, the type I reaction occurs, mainly, in anoxic environments and ^{3}PS* can transfer electrons (or protons) to oxygen or other adjacent biomolecules to form a radical anion or cation, respectively. In this type of reaction, the ^{3}PS* can react directly with an organic substrate transferring electrons (or protons), producing an oxidized substrate and reducing the PS. The reduced PS can react with molecular oxygen, producing superoxide anions.

This superoxide anion is not very reactive in a biological context, but it can be rapidly converted to form hydrogen peroxide (H_2O_2) and, consequently, form the high reactive hydroxyl radical (OH•). In the presence of metal ions, like iron or copper, superoxide anion also produces hydroxyl radicals. This cascade of process and, consequently, ROS production leads to oxidative stress and, consequently, cell death.[74, 76, 89]

1.6.3.2 Type-II photochemical reaction

When transfer of energy to molecular oxygen occurs without the transfer of an electron, it means that is occurring a type-II reaction. Usually, this reaction occurs in oxygenated environments and, as mentioned before, is reported as the main reaction during PDT.[76] Molecular oxygen has a special characteristic since the triple-state ($^3O_2$) represents the ground state of the molecule, having two unpaired electrons with parallel spins. When this transfer occurs, the $^3O_2$ is excited to singlet oxygen ($^1O_2$), a very reactive specie characterized by paired electrons, which has extremely oxidant properties. Thus, in type-II reaction the $^3PS^*$ transfers its energy to molecular oxygen in their ground-state, leading to their excitation to the very reactive $^1O_2$.[62, 74, 89]

1.7 Photodynamic therapy in Age-Related Macular Degeneration: Clinical application and state of the art

PDT has many therapeutic applications in different areas: dermatology, ophthalmology, cardiovascular, gastrointestinal, and urological disease, and several types of cancer.[90] Usually, dermatology and cancer are the most common diseases using PDT but during the end of XX century, PDT has also been gained a lot of attention in ophthalmology. PDT appeared in ophthalmology in the 1990s, with the verteporfin therapy for CNV associated with AMD and pathological myopia.[72] Since then, no other PS has been reported for use in eye disease therapy. Nevertheless, some studies and clinical applications with verteporfin were performed in others pathological contexts. The treatment of CNV associated with several retinochoroidal diseases, like choroiditis, angioid streaks and central serous chorioretinopathy, and diseases without any CNV, like choroidal hemangioma and chronic central serous chorioretinopathy, seem to have encouraging results regarding the use of PDT with verteporfin.

In AMD context, the main objective of this therapy is the selective destruction of CNV with the preservation of the overlying neurosensory retina. The PDT, in the same way as photocoagulation, can only be effective during the proliferative stage of AMD, when the neovascularization process is active. This means that, for patients with the neovascular form in an active stage, PDT can slow the progression of the disease and prevent vision loss but it cannot recover the vision already lost.[91] Currently, verteporfin is the only PS used in AMD, being restricted to the neovascular form.

Verteporfin, a reduced porphyrin derivative, is a chlorin-type molecule classified as a second-generation PS. It is synthesized from protoporphyrin and has a strong absorption peak at a wavelength of 688 nm in organic

solvents and 692 nm in aqueous solvents.[92] When irradiated, verteporfin has a high ability to generate ROS which leads to the damage of the vasculature, specially endothelial cells, resulting in vessel occlusion.[93] Clinically, verteporfin in AMD patients is administrated through intravenous injection with a usual dosage of 6 mg/m^2.[92] Firstly, there is an uptake of the PS in neovascular endothelial cells during the proliferative stages, *i.e.,* while the neovascularization process is active. After an interval of time of approximately 15 min, the irradiation is performed in the area, usually with a light dose of 50 J/cm^2 at an intensity of 600 mW/cm^2 over 83 seconds. The activation of PS leads to the generation of ROS that selectively damages neovascular endothelial cells, occluding vessels in CNV lesions.[92] After PDT treatment, the patient has to be careful with light since, due to PS accumulation, patients become extreme light-sensitive and can suffer of several adverse effects. In this sense, patients are requested to avoid direct sunlight or bright indoor light for 5 days after the treatment.[94]

One of the first studies performed in patients with CNV, where verteporfin was applied with PDT, allowed to demonstrate the safety of PDT and efficacy of the PS in CNV.[95] Indeed, PDT seems to provide an ideal treatment for neovascular AMD, since it is possible to maintain the retinal structure and adjacent tissues of CNV while occluding the pathological CNV. In this study, sixty-one patients were tested using an administrated dose of 6 mg/m^2 of verteporfin and a diode laser emitting at 690 nm with a fluence of 50 J/cm^2 to activate the PS. The complete cessation of leakage from classic CNV that usually occurs in all cases after 1 week and 50% after 4 weeks of treatment was observed. However, in 70-80% of the cases the leakage reappeared at week 12 after the treatment, but markedly less than before treatment.

In another study, the treatment of AMD with PDT study group demonstrated that PDT using verteporfin can safely reduce the risk of vision loss in patients with CNV due to AMD.[96] Six hundred nine patients were studied and randomly divided into two groups: one treated with verteporfin (6 mg/m^2) and other with placebo (5% dextrose in water) administration *via* intravenous infusion. Examination every 3 months was performed and retreatment was applied if the angiography showed leakage, with 94% of patients completing the 12th month examination and visual acuity examination. The visual acuity was evaluated using the Snellen test that uses a chart of letters or symbols, using the count of letters that a patient can see as the evaluation parameter. Both eyes were tested with different charts. In this study, the authors observed that 246 of 402 eyes assigned to verteporfin, compared to 96 of 207 eyes assigned to placebo, had lost fewer than 15 letters of visual acuity of baseline. These results showed that verteporfin therapy can safely reduce the risk of vision loss which turns verteporfin a recommended treatment.

However, during the last few years, some adverse effects associated with verteporfin treatment have been reported, such as visual disturbances, line abnormal vision, visual field defects, infusion-related pain, and photosensitivity.[94] Moreover, other serious and worrying adverse effects can occur, like vitreous hemorrhage, cataracts, retinal capillary nonperfusion, an allergic reaction, and other problems like cardiovascular, digestive, and hepatic issues. Besides this, some patients have also experienced a severe decrease in vision of 4 lines or more within 1 week after treatment with verteporfin. [94]

In sum, every therapy's approach discussed had its own particular strengths and limitations, and none offered a perfect solution or a cure of CNV associated with neovascular AMD. Nevertheless, the use of anti-VEGF

therapy with verteporfin PDT combination has been suggested recently. [97, 98] One of these studies, using verteporfin therapy and intravitreal injection of bevacizumab (combined and alone) in CNV due to AMD, concluded that there is a significant improvement in visual acuity after 1 month and their maintenance over a 3-month period after combined therapy compared with monotherapy with verteporfin PDT or anti-VEGF, bevacizumab. [98] In addition, studies with combined therapy of anti-VEGF drugs and verteporfin PDT indicated a decrease in the number of anti-VEGF injections needed, which was an advantage.[97]

1.8 Objectives

AMD is a retinal degenerative disease that can progress to the advanced two forms, dry and wet. The former is also known as geographic atrophy and corresponds to a confluent area of atrophic lesions. The latter occurs when there is the growth of abnormal vessels from the choriocapillaris which penetrate the Bruch´s membrane and the monolayer of the RPE. This can result in subretinal fibrosis. Therefore, wet AMD is characterized by both development of fibrosis and vascular proliferation. It is well-known that VEGF isoform A (VEGFA) plays a pivotal role in pathological angiogenesis, such as CNV and, RPE has been pointed as a major source of this angiogenic factor.[99, 100]

Galectin-1 belongs to the family of beta-galactoside-binding proteins and has been reported to regulate many cellular processes, including cell proliferation and cell differentiation.[36] Recently, galectin-1 has been described as a proangiogenic molecule, with a key role also in fibrosis development, in the context of neovascular AMD.[36] Gal-1, similarly to VEGF, is mainly produced by RPE cells. [36]Although Gal-1 and VEGF are two proangiogenic factors, both induced by hypoxia, they seem to act in different signaling pathways. In a laser-induced CNV animal model, Gal-1 has been identified in RPE-derived fibroblast losing melanin pigments, which proliferate, migrate and are present near new choroidal vessels.[36] Although anti-VEGF therapy is nowadays the standard treatment for the management of wet AMD, there is still a large proportion of patients without stabilization or vision improvement. In fact, multiple injections of anti-VEGF seem have negligible effect in sub-retinal fibrosis, which results from epithelial-mesenchymal transition dysfunction (EMT) and involves RPE dedifferentiation into fibroblasts-like RPE.

The main purpose of this study was to assess the cytotoxicity on ARPE-19 cells after PDT with glyco-conjugates: a free-porphyrin conjugated with four thioglucose molecules (**$H_2TPPF_{16}(SGlc)_4$**) and zinc-porphyrin conjugated with four thioglucose molecules (**$ZnTPPF_{16}(SGlc)_4$**) (**Figure 5)**. For that, we used ARPE-19 cells, which when cultured under specific conditions; they attain morphology reminiscent of fibroblasts. In this work, we proposed the evaluation of two PS, porphyrin-sugar conjugates, which will be recognized by galectins overexpressed in advanced AMD. This project may contribute for the development of new promising therapeutic agents, with enhanced photosensitizing efficacy, able to selectively destroy fibrosis and eventually CNV in wet AMD.

Based on this, the main specific objectives of this work are:

1) Study the optical absorption spectra of glyco-conjugates, already synthesized: a free-porphyrin conjugated with four thioglucose molecules and Zn-porphyrin conjugated with four thioglucose molecules
2) *In vitro* studies to evaluate the efficacy of the PS:
    a. Determine the cellular uptake by ARPE19 cells;
    b. Assess the toxicity of the conjugates in darkness and after light activation;
    c. Quantify the levels of ROS after PDT treatment

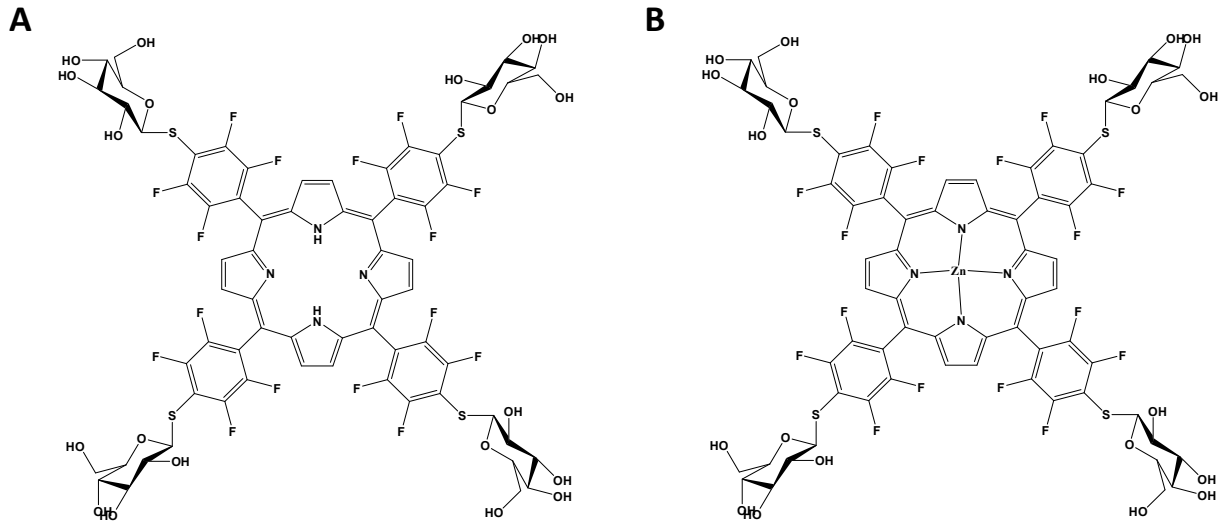

Figure 5. Chemical structure of **(A)** a free-base porphyrin, **$H_2TPPF_{16}(SGlc)_4$,** and **(B)** a zinc-porphyrin complex, **$ZnTPPF_{16}(SGlc)_4$**, both conjugated with four thioglucose units.

Chapter II
Materials and Methods

2.1 Materials and equipment

2.1.1 Equipment

The centrifuge was a SIGMA 2-16 and the microcentrifuge was a MiniFuge Galaxy MiniStar C1413. The shaker was a standard analog shaker from VWR.

To measure the UV-Visible absorbance and the fluorescence for the porphyrin-based photosensitizers was used a microplate reader Syrnergy™ HT (Biotek Instruments) controlled by BioTek's Gen5™ Data Analysis software and the microscope used was a fluorescence microscope from Zeiss (Model Axio Observer 27).

To perform the irradiation was used a LEDs array system emitting white light with two emission peaks at $\lambda = 450 \pm 20$ nm and $\lambda = 550 \pm 50$ nm, resulting in a fluence rate of 8.4 $mW.cm^{-2}$. This system is composed of a matrix of 24 x 16 LEDs which makes a total of 384 light sources emitting white light. The regulated Plug-in adaptor with LED indicator 800 mA was purchased from MW.

The Mini Protean electrophoresis system and the Mini Trans-Blot system were from Bio-Rad Laboratories. The chemiluminescence detection system used was the Chemi DocTM XRS from Bio-Rad controlled by the software Quantity One.

2.1.2 Materials

Canted neck cell culture flasks 75 cm^2 with 0.2 μm vent cap were purchased from Corning. Transparent (Orange Scientific), total black and black with transparent bottom (Greiner Bio-One) 96-wells microtiter plates for the absorbance and fluorescence studies were used. The Neubauer chamber, or hemocytometer was from VWR. The Immun-Blot PVDF membranes were purchased from Bio-Rad.

2.1.3 Buffers, reagents, KITs and chemical products

A free-porphyrin conjugated with four thioglucose molecules **($H_2TPPF_{16}(SGlc)_4$)** and Zn-porphyrin conjugated with four thioglucose molecules **($ZnTPPF_{16}(SGlc)_4$)** was synthesized and characterized by Professor Dr. João Tomé team at the Centro de Química Estrutural (CQE), Departamento de Engenharia Química, Instituto Superior Técnico, Universidade de Lisboa, Portugal.

Sodium dodecyl sulfate (SDS), Calcium Chloride (KCl), Disodium phosphate (Na_2HPO_4), Monopotassium phosphate (KH_2PO_4), dimethylsulfoxid (DMSO), 3-[4,5-dimethylthiazol-2-yl]-2,5-diphenyltetrazolium bromide (MTT) and glycine were purchased from Sigma-Aldrich. The trypan blue stain 0.4% was from BioWhittaker Reagents, Lonza. The acrylamide/Bis 20& solution was from Bio-Rad. The 2-propanol was from J.T.Baker BAKER ANALYZED™ A.C.S reagents. The hydrochloric acid (HCl) 37% was from Panreac. The

VectaSHIELD mounting medium with DAPI was purchased from VECTOR. Sodium chloride (NaCl) were from Merck. The fluorescent dye dihydroethidium (DHE) was purchased from Life Sciences.
In the BCA assay was used the Pierce BCA Protein Assay Kit-Reducing Agent Compatible (containing the BCA Protein Assay Reagent and Bovine Serum Albumin (BSA) standards at 2 $mg.mL^{-1}$) from Thermo Scientific.
The Immun-StarTM WesternCTM Chemiluminescent Kit (containing the chemiluminescent substrate: luminol/enhancer and peroxide solution) used in the western blotting assays was from Bio-Rad.
The phosphate buffered saline (PBS) buffer was prepared in Milli-Q water at pH 7.40: 137 mM NaCl, 27 mM KCl, 81 mM Na_2HPO_4, 15 mM KH_2PO_4. The 1% SDS lysis buffer was prepared with 1% (v/v) SDS in PBS buffer at a pH of 7.0.
The running buffer was prepared was prepared in Mili-Q water at pH 8.3: 25Mm Tris base, 192 mM glycine, 0.1%(m/v) SDS. The transfer buffer was prepared in the same solvent: 25 mM Tris base, 192 mM Glycine, 20% (v/v) MeOH, 0.005% (m/v) SDS. The TBST buffer was prepared with: 20 mM Tris base, 150 mM NaCl, 0.1% (v/v) Tween 20.
The primary antibodies used in western blot was: Rabbit anti-galectin 1 Monoclonal antibody, from Abcam; Mouse anti-β-Actin Monoclonal antibody, from Sigma.

2.1.4 Cells, culture medium and trypsin

In this study a human retinal pigment epithelial cell line, ARPE-19 (ATCC® CRL-2302™), isolated from retina of a male with 19 years were used. The cell medium used was DMEM:F12 medium, from ATCC, containing 10% FBS, from Gibco, and 1% (v/v) antibiotic/antimycotic containing penicillin, streptomycin and amphotericin B, from Sigma-Aldrich. The trypsin used in the cells was Trypsin-EDTA solution used was from Gibco.

2.1.5 Software

For the analysis and quantification of the images obtained in fluorescent microscope and in western blot assay was used ImageJ 1.42n (Wayne Rasband, National Institutes of Health, USA).
GraphPad Prism (v. 8.00, GraphPad Software) was used to prepare the graphs and perform the statistical analysis of the data.

2.2 Methods

2.2.1 UV-Visible characterization

The stock solutions of the PSs at a concentration of 2 mM were prepared in DMSO and stored at -20 ºC in dark conditions. The different working solutions, with different concentration of PSs were freshly prepared from the respective stock solution in sterile PBS and DMSO. The absorbances of different working solutions were scanned at wavelengths ranging from 350 to 800 nm using the plate reader.

2.2.2 Cell culture and maintenance

The ARPE-19 cells were maintained at a humidified incubator at 37 ºC and 5% carbon dioxide (CO_2) and 95% air and cultured in DMEM: F12 medium. The ARPE-19 cell line was frozen in 1 mL vials in liquid nitrogen using DMEM:F-12 medium containing 10% (v/v) DMSO. To defrosting cells the vial content was thawed in 37 ºC and transferred to 5 mL of DMEM: F12 medium. After centrifugation at 1500 rpm during 5 min, appropriate aliquots of cell suspension were added to new 75 cm^2 cell culture flasks. Cells were grown as a monolayer, at 37 ºC, in a humidified incubator grassed with 5% CO_2 and 95% air.

2.2.3 Subculturing

When ARPE-19 cells were normally 85-90% confluent in culture flasks, subculturing was necessary. For that, the culture medium was removed and discarded, and the cells were rinsed twice with warm sterile PBS in order to remove traces of serum which would inhibit the action of the trypsin. After addition of Trypsin-EDTA solution to the flask, cells were incubated at 37 ºC until the cells were in suspension and appeared rounded. After addition of regular medium to the cell suspension, a centrifugation at 1500 rpm for 5 min was performed and cells were resuspended in DMEM: F12 medium and appropriate aliquots of cells were added to new 75 cm^2 culture flasks and incubated ate 37 ºC. Normally, cells were examined carefully ever day by eye on an inverted microscope. ARPE-19 cells were subcultivated at a ratio of 1:3 to 1:5 in condition described.

2.2.4 Experiments with ARPE-19 cells

2.2.4.1 ARPE-19 cells seeding density

To prepare the cells for the treatment with PS, after the centrifugation the cells were resuspended in DMEM:F12 medium. To count cells were suspended 20 μL of cell suspension in 20 μL of trypan blue and the viable cells (bright cells) were counted using a hemocytometer.

After, the cells were plated into cell culture plated of 96-, 48- or 12- wells, depending of the assay performed, at a density of 3.0 x 10^4, 8.9 x 10^4 or 3.0 x 10^5 cells *per* well, respectively. After, the cells were maintained in an incubator at 37 ºC with 5% CO2 and 95% air and the assays were performed 24h after.

2.2.4.2 Quantification of proteins by Western Blotting

To detect and quantify specific proteins from a complex mixture of proteins extracted from cells Western Blot assay can be used. This technique is divided into three steps: separation proteins by molecular weight, by SDS-PAGE; transfer of the proteins to a membrane producing a band for each protein; and, then, incubating the membrane to mark target protein using a proper primary and secondary antibody to identify the proteins of interest. [101]

The cells were washed twice with ice-cold PBS and lysed by addition of ice-cold RIPA buffer with fresh protease inhibitors. The cold temperature and protease inhibitors are important to avoid denaturation of proteins. The cell lysates were then transferred to microtubes and incubated on ice during 30 min and vortexed 10 seconds every 10 min. After the incubation, the total cell lysates were centrifuged at 10 000 *g* during 1h, at 4 ºC. The supernatant was removed to a new microcentrifuge tube and used for protein concentration determination.

To measure the protein concentration was used the bicinchoninic acid (BCA) assay. This assay is based on two steps: the biuret reaction and after the chelation of two molecules of BCA with on cuprous ion. In the biuret reaction, there is the reduction of cupric ion (Cu^{2+}) to cuprous ion (Cu^{+}) by peptide bond in protein which results in the blue color. Based on this, it is possible to note that the amount of reduced Cu^{2+} in directly proportional to the amount of protein present in solution. After, the chelation of two molecules of BCA with on Cu^{+} results in a purple-colored product. This complex, BCA-copper, have a strong absorbance at 562 nm with increasing concentration of protein.[102] To perform this assay was used the Pierce BCA Protein Assay Kit-Reducing Agent Compatible.

In a 96-wells plate the following solutions were pipetted into each well:

- 25 μL of sample buffer: RIPA buffer;
- 25 μL of sample, sample buffer, standard;
- 200 μL of BCA working reagent: 50 parts of BCA reagent mixed with one part of BCA reagent B).

The standard were prepared in the sample buffer at concentration ranging from 12.5 to 800 $\mu g.mL^{-1}$ using the BSA standard at 2 $mg.mL^{-1}$.

After pipetted all solutions to the plate, an incubation at 37 ºC for 30 min was performed. After this, the absorbance was measured at 570 nm in the plate reader spectrophotometer. Plotting directly the average of the absorbance of each sample for each BSA standard was obtained the protein concentration in the samples ($\mu g.mL^{-1}$).

After the determination of protein concentration, the samples were denatured with 6x Laemmli buffer and heated at 95 ºC during 5 min. Then, protein samples were loaded on 10% or 12% polyacrylamide gels and the proteins were separated by electrophoresis. During this process proteins were separated by their molecular weights, and the electrophoresis was stopped when the dye front reached the bottom of the gel.

After gel electrophoresis, the protein mixture separated was transferred to a membrane, polyvinylidene difluoride membranes. Firstly, the membrane was activated with 100% of methanol, and then soaked in Milli-Q water and equilibrated in transfer buffer. In addition, all the material used in the blotting, as well as, the gels were also equilibrated in transfer buffer. The gel and the membrane were assembled into a sandwich along with sheets of filter paper and sponges, and then separated protein was transferred to the membranes for 90 min under agitation, in ice cold transfer buffer. Following the transfer, in order to avoid non-specific bonds, membranes were blocked with a 5% (w/v) non-fat milk in PBS for 1 h with agitation, at room temperature.

Then, membranes were incubated with primary antibodies, diluted in blocking buffer, overnight at 4 ºC. After the primary antibody incubation, membranes were washed every 10 min with PBS-T for 30 min at room temperature and then incubated with adequate secondary antibody with agitation for 1 h at room temperature. After incubation, membranes were washed again every 10 min with PBS-T for 30 min. In the end, the intensity of the bands was detected on the chemiluminescence detection system, incubated with the substrate solution, mixture of luminol/enhancer and peroxide buffer (1:1, by volume).

2.2.4.3 Preparation of PS working solutions

The stock solutions of the PSs at a concentration of 2 mM were prepared in DMSO and stored at -20 ºC in dark conditions. The working concentrations of PSs are freshly prepared in sterile PBS. The concentration of DMSO was always lower or equal to 0.5% (v/v) in all working solutions.

2.2.4.4 Treatment of ARPE-19 cell line with photosensitizer

One day after seeding the cells into multiwell plates, the culture medium (DMEM: F12) was removed and cells were incubated with increasing concentrations and various periods of time of PSs in dark conditions. After incubation, the PS solution was removed and the cells were washed with warm and sterile PBS in order to remove the excess of PS.

2.2.5 Determination of intracellular concentration of photosensitizer by fluorimetry

Based on the fluorescence properties of the porphyrins, it is possible to determine the amount of PSs accumulated in cells by fluorimetry. After assessment of intracellular amount of photosensitizer by fluorimetry, the data were normalized to total protein quantity.

After the PSs incubation, the cells were washed twice with sterile PBS. Cells were mechanical scrapped in 120 µL of 1% (m/v) SDS solution in PBS with pH = 7.0. 90 µL of this cell suspension were transferred to 96-wells black plates and the intracellular fluorescence of the PSs was determined by fluorometric measurement, using a set of standard solutions with known concentrations of PS for creation of a calibration curve. For this type of PSs, porphyrin-based PSs, the intracellular fluorescence was determined using the plate reader fluorometer and the excitation and emission filters used were 360/40 nm and 645/40 nm, respectively. The PS concentration in sample was directly obtained by plotting the average of the fluorescence for each PS standard in function of its concentration (µM).

To measure the protein concentration was used the BCA assay, using the Pierce BCA Protein Assay Kit-Reducing Agent Compatible, follow the same protocol described before in Western Blot, with some differences once the samples were in 1% (m/v) SDS in PBS (7.0).

In a 96-wells plate the following solutions were pipetted into each well:

- 25 µL of sample buffer: 1% (m/v) SDS in PBS (pH 7.0);
- 25 µL of sample, sample buffer, standard;
- 200 µL of BCA working reagent: 50 parts of BCA reagent mixed with one part of BCA reagent B).

The standard were prepared in the sample buffer at concentration ranging from 12.5 to 800 $\mu g.mL^{-1}$ using the BSA standard at 2 $mg.mL^{-1}$.

After pipetted all solutions to the plate, an incubation at 37 ºC for 30 min was performed. After this, the absorbance was measured at 570 nm in the plate reader spectrophotometer. Plotting directly the average of the absorbance of each sample for each BSA standard was obtained the protein concentration in the samples ($\mu g.mL^{-1}$).

2.2.6 Photodynamic assays

In PDT it is important to be sure that the PSs produce toxicity just after activation by light, and they do not induce any toxicity or just a minimal toxicity in darkness. Based on this, it is important to evaluate the PS toxicity under two conditions: in the absence of light and after light irradiation. After PSs incubation, the cells were washed with warm and sterile PBS and covered with fresh DMEM: F12 medium.

To perform the irradiation, the plate was placed above the LEDs array system emitting white light and the cells were irradiated for 40 min in a dark room and after this were incubated, in darkness, during 24h in the humidified incubator with 5% CO_2 and 95% air.

2.2.7 Cell viability assays

2.2.7.1 MTT colorimetric assay

MTT, yellow colored, when added to living cells is reduced to an insoluble formazan, with a blue purple color, by a mitochondrial enzyme succinate dehydrogenase. [103] Based on this, it is possible to evaluate the cellular viability through the MTT reduction.

The cells were carefully plated into 96-multiwell plate at a density of 3.0 x 10^4 cells *per* well, treated with PS and then performing the photodynamic assays as described before. Twenty-four hours after the photodynamic treatments, 150 µL of the DMEM: F12 medium was removed and added 10 µL of MTT stock solution at concentration of 3 mg. mL^{-1} in sterile PBS buffer to each well. The plates were then incubated in the darkness at 37 ºC for 4 h. During this time was formed purple needle-shaped crystal's and then dissolved in 150 µL of acid isopropanol (0.04 M HCl in absolute isopropanol). Then, using a microplate reader spectrophotometer, the absorbance was measured at 570 and 620 nm. The percentage of absorbance for each treated sample was normalized to that of the respective untreated control cells and the results were expressed as percentages of MTT reduction according the following calculations:

For each well, the absorbance was expressed as the difference between the two absorbances (absorbance 570 nm – absorbance 620 nm). The, three MTT reduction was calculated:

$$\boldsymbol{MTT\ reduction}\ (\%) = \frac{\boldsymbol{Absorbance\ treated\ samples}}{\boldsymbol{Absorbance\ control\ samples}} * \mathbf{100}\ \%$$

2.2.7.2 Trypan blue assay

Trypan blue is an organic amine dye and their exclusion is used to determine the number of viable cells. Live cells possess intact cell membranes which allows to exclude certain dyes, like trypan blue. On the other hand, death cells will take up trypan blue. So, this assay allows to count the number of live cells, clear cytoplasm, and dead cells, blue cytoplasm, under a microscope. [104]

The cells were carefully plated into 48-multiwell plate at a density of 9.8 x 10^4 cells *per* well. treated with PS and performed the photodynamic assays as described before. Twenty-four hours after the photodynamic

treatments, the culture medium of each well was removed to an Eppendorf and was added the Trypsin-EDTA solution until the cells rounded up and the cell layer begun being dispersed. After, the cells suspension in Trypsin-EDTA solution was added into the Eppendorf with culture medium and centrifuged at 1500 rpm during 5 min in a microcentrifuge. The supernatant was removed and the cells were resuspended in DMEM: F12 medium. After the cell's suspension was diluted in trypan blue and the cells were counted as explained before. The viability was calculated as follows:

$$\textbf{\textit{Viable cells}}\ (\%) = \frac{\textbf{\textit{Number of viable cells}}}{\textbf{\textit{Number of total cells}}} * \mathbf{100}\ \%$$

2.2.8 Determination of reactive oxygen species (ROS) levels

The detection of ROS, like superoxide anions, hydroxyl radicals, hydrogen peroxide, nitric oxide, peroxynitrite and single oxygen, was done by fluorescent dyes. In the present work, we used dihydroethidium (DHE) dye, which when inside the cells and in the presence of ROS, is oxidized by ROS (particularly superoxide anion) to a specific red fluorescent 2-hydroxyethidum, which intercalates within the cell's DNA, staining in the nucleus with bright red fluorescence. The generation of ROS by this probe can be evaluated by fluorescence microscopy and fluorescence spectroscopy techniques.

2.2.8.1 ROS quantification by fluorescence microscopy

The ARPE-19 cells were plated carefully in coverslips at a density of $3.0*10^5$ cells per well, in 12-wells culture plated for 24 h before treatment. After PSs and photodynamic treatment, cells were incubated with 5 μM of dye for 30 min at 37 ºC, in dark conditions. Then the cells were washed in PBS and fixed in 4% PFA for 10 min at room temperature. The samples were washed with PBS, tree times during 5 min. The coverslips were mounted using the VectaSHIELD mounting medium, sealed with nail polish and stored at 4 ºC until visualization under the fluorescence microscope.

2.2.8.2 ROS quantification by fluorimetry

The 96-wells culture black plate were coated with poly-L-lysine (diluted 1:10, by volume in sterile PBS) ARPE-19 were plated at a density of $3.0*10^4$ cells *per* well, in 96-wells culture black plate for 24 h before treatment. After PSs and photodynamic treatment, as described early. The cells were incubated, in darkness, with 5 μM of DHE in PBS for 30 min at 37 ºC after PSs and photodynamic treatment performed. Then, fluorometric measurement was performed with the appropriate excitation and emission filters to probe (485/20 nm and

590/35 nm to DHE). The intracellular fluorescence of probes was normalized to total protein quantity through BCA assay.

Chapter III
Results

3.1 α-SMA and galectin-1 are expressed in ARPE-19 cells

Under specific conditions, such as a short time in culture, ARPE-19 cells can acquire morphology reminiscent of fibroblasts **(Figure 6 A).** In fact, these cells were shown to express α-smooth muscle actin (α-SMA), which is a marker of differentiated fibroblasts (myofibroblasts) **(Figure 6 B).** Moreover, these cells also present galectin-1 protein **(Figure 6 B).** This sugar-binding protein can increase the specificity/uptake of the PSs used in this study, which are coupled to thioglucose molecules.

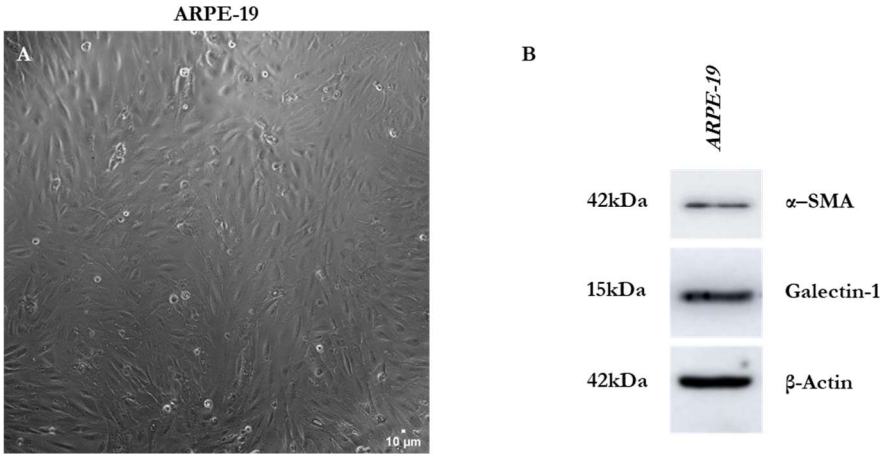

Figure 6. (A) ARPE-19 cells present a reminiscent morphology of fibroblasts; **(B)** ARPE-19 cells present α-SMA, a marker of fibroblasts, and galectin-1. β-actin was used as a control loading in the Western blot analysis.

3.2 UV-Visible characterization

The absorption spectra of **$H_2TPPF_{16}(SGlc)_4$** and **$ZnTPPF_{16}(SGlc)_4$ (Figure 7)** were acquired both in DMSO and PBS solution with 0.5% of DMSO. Both compounds at a concentration of 2 µM in DMSO, presented an intense peak attributed to the Soret band, located at 415 and 423 nm for **$H_2TPPF_{16}(SGlc)_4$** and **$ZnTPPF_{16}(SGlc)_4$**, respectively. Besides, Q-bands were identified around 510 and 583 nm for **$H_2TPPF_{16}(SGlc)_4$** and 550 nm for **$ZnTPPF_{16}(SGlc)_4$**. Their absorption spectra were also acquired in PBS with 0.5% of DMSO at the same concentration and show an intense peak, Soret band, at 411 e 420, respectively, and Q-bands around 512 nm and 585 nm, for **$H_2TPPF_{16}(SGlc)_4$**, and around 555 nm for **$ZnTPPF_{16}(SGlc)_4$.**

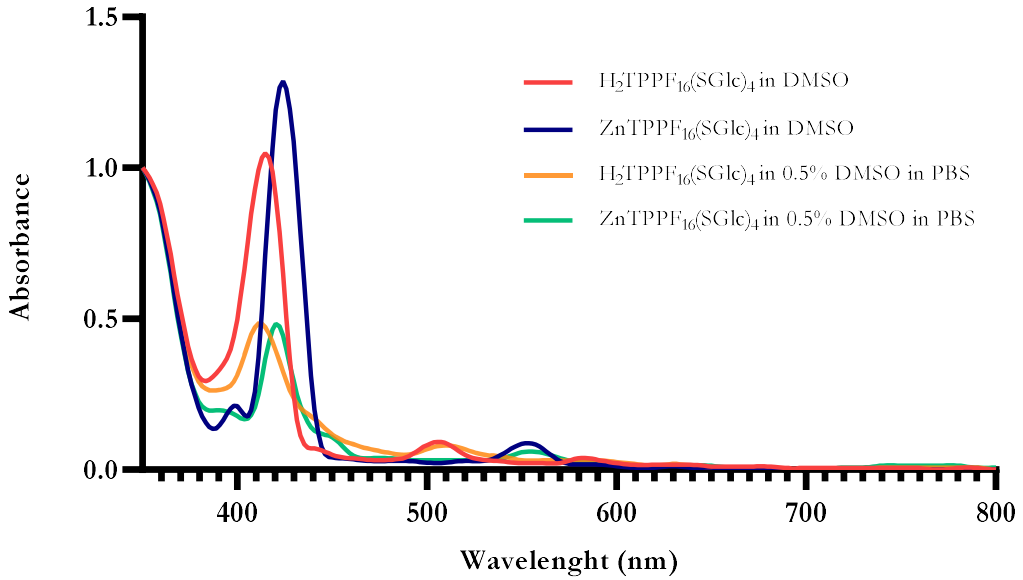

Figure 7. Electronic absorption spectra of **H_2TPPF$_{16}$(SGlc)$_4$** and **ZnTPPF$_{16}$(SGlc)$_4$** at 2 μM in DMSO and PBS with 0.5% of DMSO.

3.3 Cellular uptake of H_2TPPF$_{16}$(SGlc)$_4$ and ZnTPPF$_{16}$(SGlc)$_4$ by ARPE-19 cells

The cellular uptake of **H_2TPPF$_{16}$(SGlc)$_4$** and **ZnTPPF$_{16}$(SGlc)$_4$** by ARPE-19 cells, was evaluated through their fluorescence properties. The cells were incubated in the absence of light at various periods of incubation time (0.5, 1, 2 and 4 h) with increasing concentrations (0.5, 1.25, 2.5, 5 and 10 μM) of **H_2TPPF$_{16}$(SGlc)$_4$** and **ZnTPPF$_{16}$(SGlc)$_4$** in PBS with the concentration of DMSO always equal to 0.5% (v/v).

According to the results **(Figure 8)**, the uptake profile of **H_2TPPF$_{16}$(SGlc)$_4$** and **ZnTPPF$_{16}$(SGlc)$_4$** by the cells was both concentration- and time-dependent. During the first 2 h, occurred the fastest uptake and after that seemed to occur a slower steady increasing, reaching a plateau. Looking to the results is possible to note that the cellular uptake of **ZnTPPF$_{16}$(SGlc)$_4$** was higher than the uptake of **H_2TPPF$_{16}$(SGlc)$_4$** by ARPE-19 cells. For example, after 2 h of incubation with **H_2TPPF$_{16}$(SGlc)$_4$** at 5 μM resulted in an uptake of 5.33 ± 1.02 nmol *per* mg protein inside the cells while the incubation with **ZnTPPF$_{16}$(SGlc)$_4$** in the same conditions, resulted in an uptake of 18.8 ± 1.26 nmol *per* mg protein.

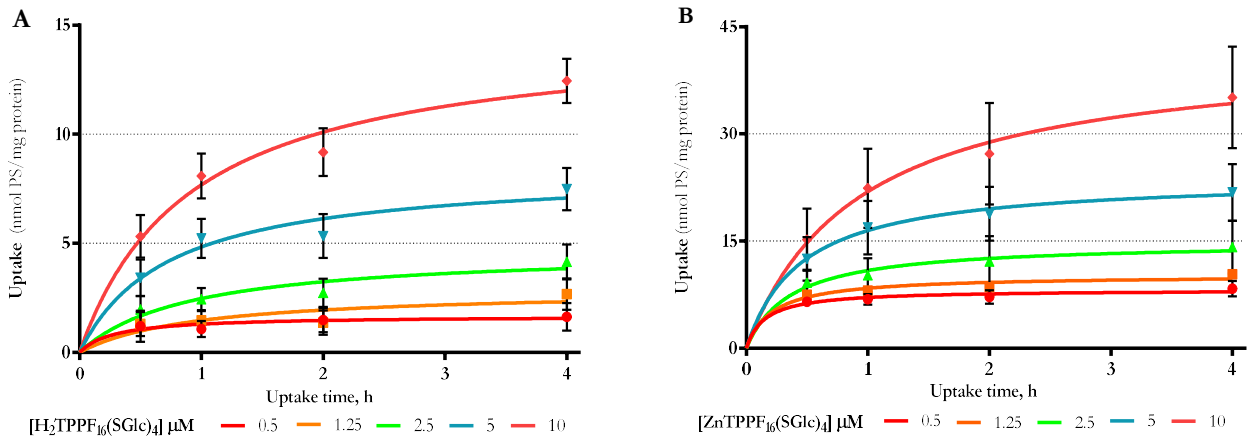

Figure 8. Cellular uptake of **(A) $H_2TPPF_{16}(SGlc)_4$** and **(B) $ZnTPPF_{16}(SGlc)_4$** by ARPE-19 cells at various concentrations (0.5, 1.25, 2.5, 5 and 10 µM) in function of the uptake time (0.5, 1, 2 and 4 h). **(A) $H_2TPPF_{16}(SGlc)_4$** and **(B) $ZnTPPF_{16}(SGlc)_4$** concentration was determined using fluorescence spectroscopy and the results were normalized to protein quantity. Data are the mean ± SEM of at least three independent experiments performed in triplicates.

3.4 Dark toxicity and phototoxicity of $H_2TPPF_{16}(SGlc)_4$ and $ZnTPPF_{16}(SGlc)_4$ in ARPE-19 cells

After confirmation of **$H_2TPPF_{16}(SGlc)_4$** and **$ZnTPPF_{16}(SGlc)_4$** uptake by ARPE-19 cells, the toxicity of both PSs was evaluated in the dark and after photoactivation. Both compounds were incubated in ARPE-19 cells in the same condition of uptake assay, with increasing incubation time (0.5, 1, 2 and 4 h) and concentrations (0.5, 1.25, 2.5, 5 and 10 µM). The cells viability was determined 24 h after treatment by MTT colorimetric assay. According to the obtained results **(Figure 9)**, the incubation concentration up to 10 µM and uptake time up to 4 h of **$H_2TPPF_{16}(SGlc)_4$** and **$ZnTPPF_{16}(SGlc)_4$** did not induce dark toxicity.

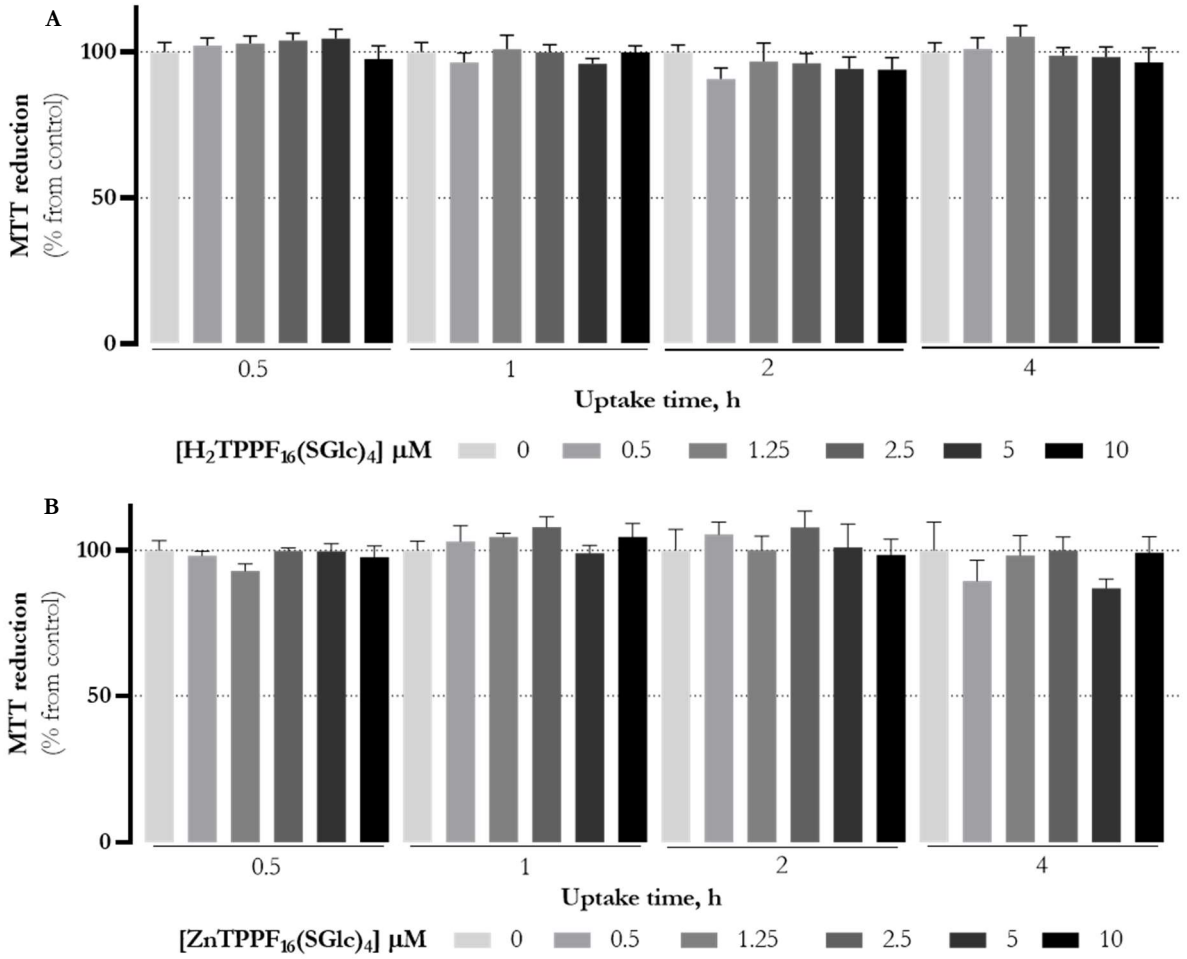

Figure 9. Non-dark toxicity of **(A) $H_2TPPF_{16}(SGlc)_4$** and **(B) $ZnTPPF_{16}(SGlc)_4$** by ARPE-19 cells. Cells were incubated with **$H_2TPPF_{16}(SGlc)_4$** and **$ZnTPPF_{16}(SGlc)_4$** at various concentration (0.5, 1.25, 2.5, 5 and 10 µM) for increasing uptake times (0.5, 1, 2 and 4 h) in dark conditions. Cytotoxicity was assessed using MTT colorimetric assay 24 h after treatment. The percentage of cytotoxicity was calculated relatively to control cells (cells incubated with PBS in darkness) at the respective uptake time. Data are the mean value ± SEM of at least three independent experiments performed in triplicates.

Once proven that both PSs did not induce toxicity in darkness, the phototoxicity, which is the toxicity after PDT treatment, was studied. In the same conditions of the previous results, namely incubation time (0.5, 1, 2 and 4 h) and concentration (0.5, 1.25, 2.5, 5 and 10 µM), after the PSs treatment, ARPE-19 cells were irradiated with white light at a potency of 8.4 $mW.cm^{-2}$ during 40 min. The cell viability was assessed by MTT colorimetric assay after 24 h of PDT treatment.

Looking to the results **(Figure 10)**, the incubation with **$H_2TPPF_{16}(SGlc)_4$** or **$ZnTPPF_{16}(SGlc)_4$** followed PDT treatment in ARPE-19 cells resulted both in a significant decrease of MTT reduction, meaning a decrease in cellular viability in a concentration- and incubation time-dependent manner.

After PDT with **$H_2TPPF_{16}(SGlc)_4$ (Figure 10 A)**, a statistically significant decrease in MTT reduction was observed when the PS was incubated at a concentration of 10 μM during 0.5, 1, 2 and 4 h, 5 μM during 2 and

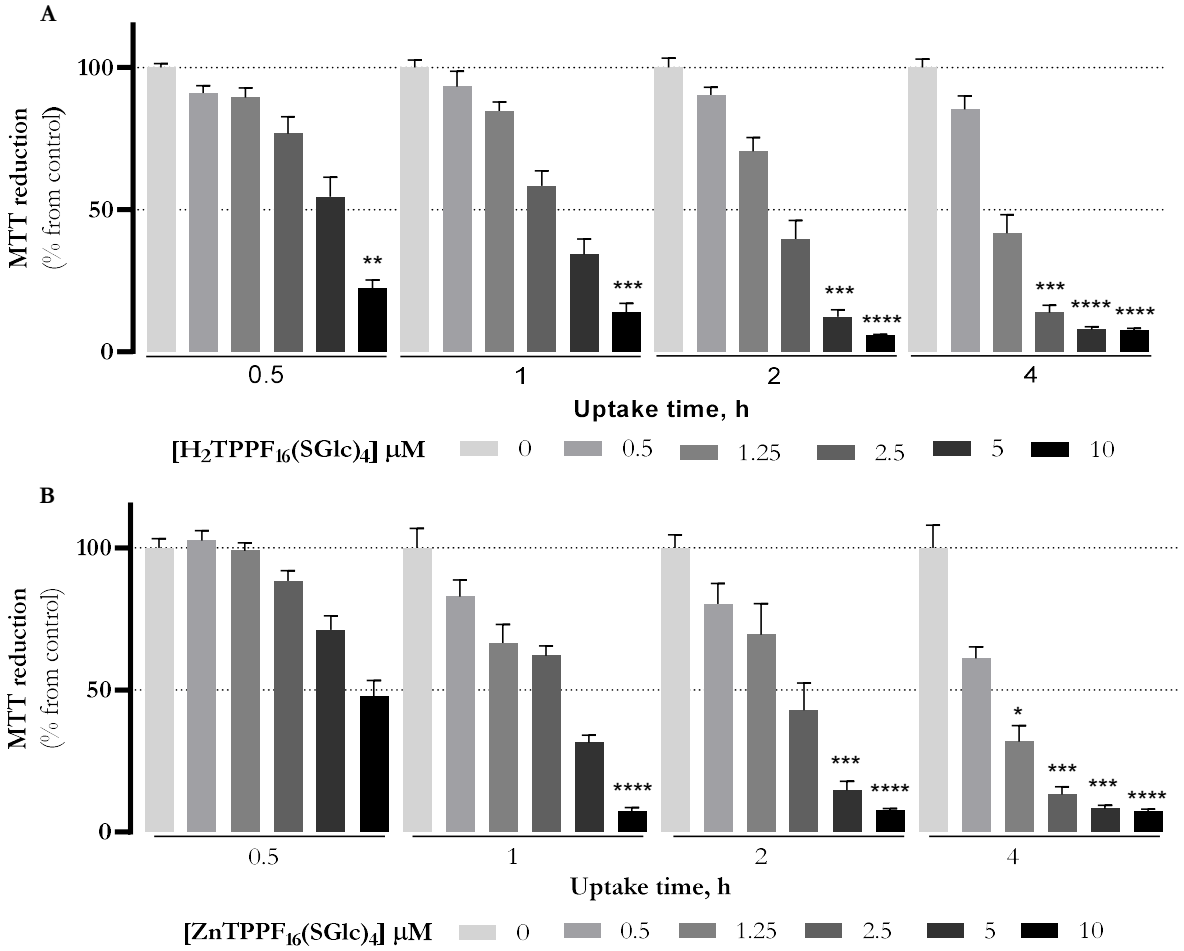

Figure 10. Photocytotoxicity effects of PDT with **(A) $H_2TPPF_{16}(SGlc)_4$** and **(B) $ZnTPPF_{16}(SGlc)_4$** by ARPE-19 cells. Cells were incubated in dark conditions with **$H_2TPPF_{16}(SGlc)_4$** and **$ZnTPPF_{16}(SGlc)_4$** at various concentration (0.5, 1.25, 2.5, 5 and 10 μM) for increasing uptake times (0.5, 1, 2 and 4 h) and irradiated with light at a fluence rate of 8.4 mW.cm-2 during 40 min. Cytotoxicity was assessed using MTT colorimetric assay 24h after PDT treatment. The percentage of photocytotoxicity was calculated relatively to control cells (cells incubated with PBS and then irradiated) at the respective uptake time. Data are the mean value ± SEM of at least three independent experiments performed in triplicates. Statistical differences were evaluated by Kruskal-Wallis test. *($p<0.05$), **($p<0.01$), ***($p<0.005$) and ****($p<0.001$) vs Control (incubated with PBS and irradiation during the same time) at the respective uptake time.

4 h and 2.5 μM during 4 h, when compared to the appropriate controls. On the other hand, PDT with **$ZnTPPF_{16}(SGlc)_4$ (Figure 10 B)** induced a statistically significant decrease in MTT reduction for the incubation of PS at 10 μM during 1, 2 and 4 h, 5 μM during 2 and 4 h and 1.25 and 2.5 μM during 4 h.

Theoretically, the MTT assay is dependent of the cell metabolism to reduce MTT in formazan. In order to confirm the toxicity induced by both compounds, we performed trypan blue assays.

The cells were incubated with **$H_2TPPF_{16}(SGlc)_4$** or **$ZnTPPF_{16}(SGlc)_4$**, in darkness or irradiated, with the same increasing concentration (0.5, 1.25, 5 and 10 μM) during 2 h. The trypan blue assay was performed 24 h after the photodynamic effects. As expected, in the absence of light **(Figure 11 A e B)** compared to the control

(incubated with PBS during the same time) there is no significant differences. However, the results after PDT treatment **(Figure 11 C e D)** presented a statistically significant decrease in exclusion of trypan blue with the incubation of 5 and 10 μM for both PSs, which revealed a decrease in cellular viability statistically significant in this concentration during this uptake time. These results were in agreement with those obtained by the MTT colorimetric assay.

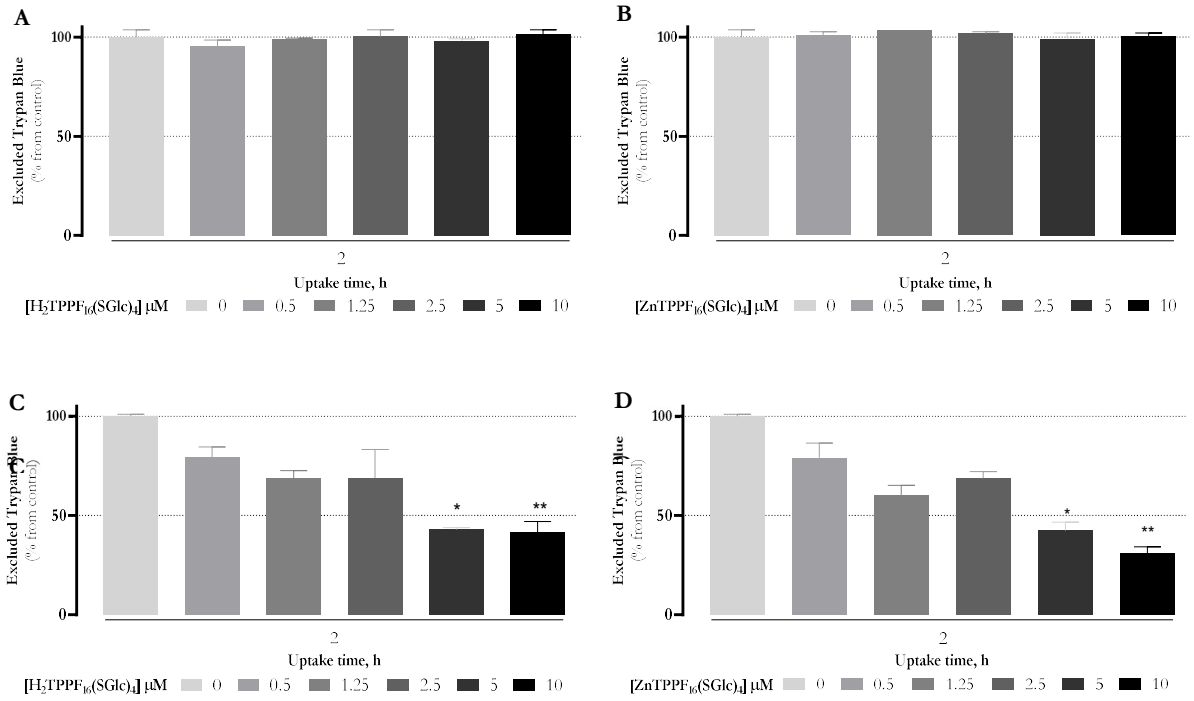

Figure 11. Non-dark toxicity of **(A) $H_2TPPF_{16}(SGlc)_4$** and **(B) $ZnTPPF_{16}(SGlc)_4$** and photocytotoxicity effects of PDT with **(C) $H_2TPPF_{16}(SGlc)_4$** and **(D) $ZnTPPF_{16}(SGlc)_4$** in ARPE-19 cells. Cells were incubated in dark conditions with **$H_2TPPF_{16}(SGlc)_4$** and **$ZnTPPF_{16}(SGlc)_4$** at various concentration (0.5, 1.25, 2.5, 5 and 10 μM) for 2 h. Cytotoxicity was assessed using trypan blue staining 24 h after photodynamic assays (in darkness or after irradiation with light at a fluence rate of 8.4 $mW.cm^{-2}$ during 40 min. The percentage of toxicity was calculated relatively to control cells (cells incubated with PBS) at the respective uptake time. Data are the mean value ± SEM of at least one independent experiment performed in triplicates. Statistical differences were evaluated by Kruskal-Wallis test. *($p<0.05$), **($p<0.01$) vs Control (incubated with PBS) at the respective uptake time.

3.5 ROS levels generated by $H_2TPPF_{16}(SGlc)_4$ and $ZnTPPF_{16}(SGlc)_4$ after PDT in ARPE-19 cells

The photodynamic effect induced by PDT treatment with PSs is due to the generation and accumulation of ROS which promote oxidative stress and, consequently, cell death. In order to confirm the generation of ROS due to **$H_2TPPF_{16}(SGlc)_4$** and **$ZnTPPF_{16}(SGlc)_4$** activation, the levels of ROS after PDT treatment were

evaluated using the DHE fluorescent dye. The red fluorescent products were identified by fluorescence microscopy and quantified by fluorimetry.

ARPE-19 cells were incubated in darkness for 2 h with PBS (control), 5 μM of **$H_2TPPF_{16}(SGlc)_4$** or **$ZnTPPF_{16}(SGlc)_4$** and then irradiated for 40 min. The images obtained by fluorescent microscopy **(Figure 12 A)** demonstrated for both compounds an increase of intracellular DHE fluorescence compared to control cells, and, when comparing both PS, was possible to note an increase in fluorescence with **$ZnTPPF_{16}(SGlc)_4$** treatment. The quantification of fluorescence intensity of the images **(Figure 12 B e C)** demonstrated a significant increase in fluorescence meaning an increase of ROS levels for both PSs. To **$H_2TPPF_{16}(SGlc)_4$** incubation there is an increase of 36.02% compared to control and **$ZnTPPF_{16}(SGlc)_4$** an increase of 84.83% compared to control.

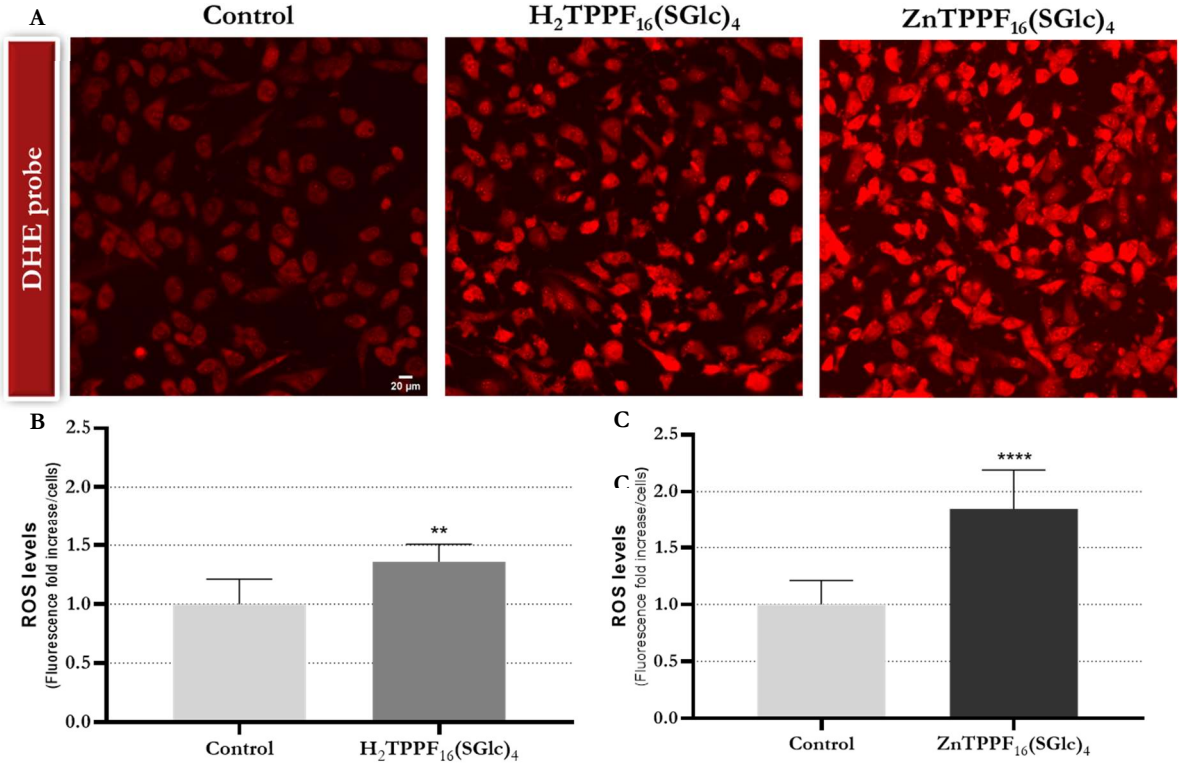

Figure 12. (A) Representative fluorescence images and respective quantification of DHE fluorescence increase (as a measure of ROS production) after **(B) $H_2TPPF16(SGlc)_4$** and **(C) $ZnTPPF_{16}(SGlc)_4$** incubation and PDT treatment in ARPE-19 cells. Cells were incubated with PBS (Control) or 5 μM of **$H_2TPPF_{16}(SGlc)_4$** or **$ZnTPPF_{16}(SGlc)_4$** for 2h in darkness. After PDT during 40 min and probe incubation, the images were acquired on a fluorescence microscope and the quantification of increase fluorescence was calculated relatively to the number of cells. Data are the mean value ± SEM of at least one independent experiment performed in triplicates. Statistical differences were evaluated by Mann-Whitney test. **($p<0.01$), ****($p<0.001$) vs Control (incubated with PBS during 2 h).

Additionally, quantitative analysis trough fluorimetry **(Figure 13)** was performed. As expected, a significant increase of ROS levels after **$H_2TPPF_{16}(SGlc)_4$** or **$ZnTPPF_{16}(SGlc)_4$** incubation was also observed, compared to control.

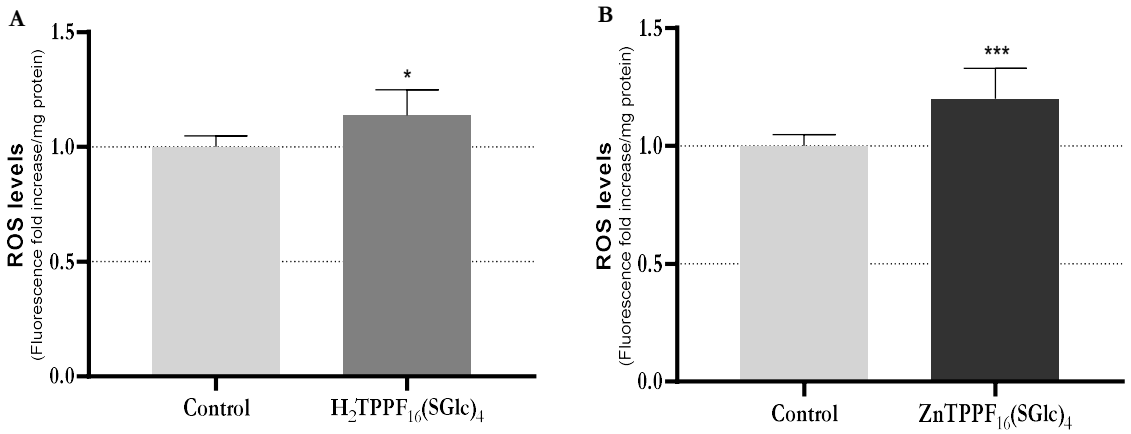

Figure 13. Quantification of DHE fluorescence increase (as a measure of ROS production) after **(A) H_2TPPF16(SGlc)$_4$** and **(B) ZnTPPF$_{16}$(SGlc)$_4$** incubation and PDT treatment in ARPE-19 cells with incubation of 5 μM of DHE. Cells were incubated with PBS (Control) or 5 μM of **H_2TPPF$_{16}$(SGlc)$_4$** or **ZnTPPF$_{16}$(SGlc)$_4$** for 2h in darkness and irradiated with light at a fluence rate of 8.4 mW.cm^{-2} during 40 min. The ROS levels was determined using fluorescence spectroscopy and the results were normalized to protein quantity. Data are the mean value ± SEM of at least two independent experiments performed in quadruplicates. Statistical differences were evaluated by Mann-Whitney test. *($p<0.05$), ***($p<0.001$) vs Control (incubated with PBS during 2 h).

Chapter IV
Discussion

4.1 Discussion

PDT is a promising modality, which is both minimally invasive and minimally toxic. It has been used in the treatment of several diseases and disorders. This therapy involves the use of PSs, which ideally would accumulate in target cells, followed by local irradiation. This leads to PSs activation and production of ROS and, consequently, tissue damage, while the adjacent normal tissues are spared. The efficiency of the PDT is mainly dependent on the selective cellular uptake of PS, its subcellular localization and capacity to generate ROS after being activated.[62] The PSs chemical structure play a role in this PDT aspects. As discussed before, chemical modification, such as bioconjugation and metalation, in PS structures can be an advantage on improving selectivity, as well as, PDT effectiveness.[80, 105] In previous works of our group, the bioconjugation of PSs with galactose has been revealed an interesting approach in the field of target cancer PDT since it allows to increase the local concentration of PSs in tumor tissues where there is an overexpression of some lectins, such as gal-1.[106]

Over the years, a wide range of PS has been conjugated with different metals cations, mainly of transition metals, for improving therapy effectiveness. Copper(II), cobalt(II), iron(II), and zinc(II) are some examples of ions used. ROS generation, such as singlet oxygen, plays an important role in the success of a specific photosensitizer in PDT. The capacity to undergo ISC during PDT reaction, the triplet quantum yield and the lifetime of PSs are directly related to ROS generation, and consequently, PDT efficacy. The insertion of certain metals in PSs structures have the capacity of enhance ISC and have a long triplet lifetime.[105] Some studies with zinc(II) complexed porphyrins show an increased cell uptake and binding to the cell membrane leading to an enhancement of the efficacy of PDT.[107, 108] Among them, Zn-porphyrins exhibit better triplet excited state quantum yield and singlet oxygen generation yield, when compared to free-porphyrins, which could be correlated with the greatest phototoxicity seen with zinc-porphyrins, improving the PDT effectiveness. [107, 109]

Based on this and in the previous studies performed by our group, two PSs were evaluated as photosensitizers, a free-porphyrin (**$H_2TPPF_{16}(SGlc)_4$**) and a Zinc-porphyrin (**$ZnTPPF_{16}(SGlc)_4$**), with four molecules of thioglucose. In the context of AMD, our interest in the use of these PSs is based on their potential recognition by Gal-1, whose levels are increased in fibrosis and choroidal neovessels in advanced AMD. This could represent a unique opportunity to selectively destroy both fibrosis and CNV by targeted PDT.

Treatment of advanced wet AMD is based mostly in anti-VEGF drugs. Sometimes, PDT with verteporfin can be used in combination with anti-VEGF therapies. Although PDT with verteporfin is able to destroy CNV. So far, any available treatment can prevent or treat subretinal fibrosis. Moreover, it has been reported that fibrosis may develop after treatment with anti-VEGF drugs in AMD.[29, 110] Fibrosis is defined as an excessive wound healing response, that has gone out of control, to tissue injury.[29, 111] Repair of damaged tissues is a fundamental mechanism for cell survival and it is a biological process that allows the replacement of dead or damaged cells. Normally, this process is divided into two stages: firstly, a regenerative stage, in which the damaged cells are replaced by healthy cells of the same type, and then a stage known as fibrosis, where connective tissue replaces normal parenchymal tissue. When out of control, it can become pathogenic leading to a substantial remodeling

of the extracellular matrix and the formation of permanent scar tissue.[111] The angiogenic process is initiated to increase the oxygen supply and recruit inflammatory cells to help in the repair of damage tissue. In neovascular AMD, CNV leads to hemorrhage and exudative changes in subretinal space, and, consequently, subretinal fibrosis.

After tissue lesion, epithelial cells, release mediators that recruit and activate inflammatory cells, endothelial cells, and fibroblasts. In addition, cells undergo EMT, being partially and transiently dedifferentiated, leading to the conversion of epithelial cells to mesenchymal cells, such as myofibroblasts.[111, 29, 112] RPE is a highly polarized monolayer of pigmented cells, between the neural retina and the choroid. During CNV, occurs RPE detachment and dissociation, disrupting cell-cell contact, and consequently, EMT. RPE cells lose their epithelial phenotype and gain mesenchymal properties. [29, 113]

Gal-1 is mainly produced by RPE cells and, recently, has been described as a proangiogenic molecule, with a key role in CNV and, also in fibrosis development, in the context of neovascular AMD. In that study, in a laser-induced CNV model (an animal model of neovascular AMD), Gal-1 has been identified in RPE-derived fibroblasts losing melanin pigments and it has been demonstrated that a deficiency in the gene that encodes Gal-1, LGALS1, led to significant suppression of CNV-associated subretinal fibrosis. Supporting the *in vivo* results, *in vitro* studies in human RPE cells with silencing of LGALS1 inhibited EMT, and, conversely, overexpression of Lgals1 enhance CNV and subretinal fibrosis. Besides this, specimens from patients with AMD demonstrated colocalization of Gal-1 in neovascular endothelial cells and RPE cells. Based on the showed results, this study suggests a biological significance of galectin-1 as a key promotor for both CNV and subretinal fibrosis via EMT in eyes with AMD.[114]

In the present work, the efficacy of **$H_2TPPF_{16}(SGlc)_4$** and **$ZnTPPF_{16}(SGlc)_4$** as PDT agents was assessed using a human RPE cell line (ARPE-19 cell line). The human RPE cell-line ARPE-19 is commonly used as an alternative to primary RPE in many studies. However, the native RPE characteristics by ARPE-19 cells depends on how they are cultured and passaged. ARPE-19 cells are cultured in DMEM with 10% FBS and, initially, they attain morphology reminiscent of fibroblasts and remain in this morphology for more than 2 weeks under these culture conditions. Studies showed that the cells only exhibit characteristics of RPE, such hexagonal morphology and an increase in pigmentation for more than 1 month. [115] So, in this work, ARPE-19 cells were used as a model of fibroblasts, which were cultured under specific conditions to attain morphology reminiscent of fibroblasts, mimicking EMT and what occurs biologically in the ocular pathology, AMD.

Firstly, as expected, we have shown that α-smooth muscle actin (α-SMA) is expressed in ARPE-19 cells. When EMT occurs, RPE cells lose their epithelial phenotype with a decrease in expression of some markers such as zonula-occludens protein-1, ZO-1, and gain mesenchymal properties with increased expression of mesenchymal markers, such as α-SMA (marker of myofibroblasts).[29] The presence of α-SMA in ARPE-19 suggests that EMT occured in ARPE-19 cells, being therefore a good model to test our PS, once fibroblasts are known to be implicated in driving biomaterial-mediated fibrosis in AMD.

Once Gal-1 seems to be have an important role in CNV and subretinal fibrosis, and taking account that PSs used in this project have the objective of being recognized by galectins overexpressed in advanced AMD, we confirmed the presence of galectin-1 in ARPE-19 cells.

As stated before, a free-porphyrin **$H_2TPPF_{16}(SGlc)_4$** and a metalled-porphyrin **$ZnTPPF_{16}(SGlc)_4$** were studied**.** Firstly, the optical absorption spectra of both PSs previously synthesized, were performed in DMSO and in PBS with 0.5% of DMSO. Both porphyrins, show intense Soret bands with respective peak maximum at 415 nm and 423 nm in DMSO and 411 e 420 nm in PBS with 0.5% of DMSO, which correspond to a strong transition to the second excited state ($S_0 \rightarrow S_2$). **$H_2TPPF_{16}(SGlc)_4$** shows two weak Q bands with the absorption maximum of 510 nm and 583 nm in DMSO and 512 nm and 585 nm in PBS with 0.5% of DMSO. With zinc in the porphyrin center, the increase structural symmetry reduces the number of Q-bands to one, at 550 nm in DMSO and 555 nm in PBS with 0.5% of DMSO. The Q-bands are resulting from a weak transition to the first excited state ($S_0 \rightarrow S_1$).

The *in vitro* assays in ARPE-19 cells with morphology reminiscent to fibroblasts were performed to evaluate cellular uptake of **$H_2TPPF_{16}(SGlc)_4$** and **$ZnTPPF_{16}(SGlc)_4$**. According to the results, the cellular uptake for both compounds by ARPE-19 cells was both concentration- and time-dependent. These results are consistent with previous work of our group, in which that this type of PS showed an increased uptake in cancer cells that overexpressed Gal-1.[106, 83] Looking to the results, it is possible to note, a slight higher cellular uptake of **$ZnTPPF_{16}(SGlc)_4$** suggesting that zinc presence potentially may favor cellular uptake in ARPE-19 cells. Zinc is an essential cofactor for normal cell function and, normal ocular tissues contain relatively high levels of zinc, mainly in the photoreceptors and RPE cells. In fact, reports showed that most of the Zn transporter is expressed in human RPE. This may indicate that **$ZnTPPF_{16}(SGlc)$** may interact with Zn transporter present in ARPE-19 cells, contributing to its higher cellular uptake. [116] The zinc is complexed in porphyrin center, however there may be some axial interaction with zinc by amino groups of proteins. Besides this, some studies with free-porphyrins and Zn-porphyrins in HeLa cells, have shown that Zn-porphyrins have the highest global uptake. In this study, this result was attributed to the higher complexing effect of zinc with phosphate groups of the phospholipids present in cellular membrane.[117] Based on the obtained results, it would be important, in the future, to validate these results with microscopy fluorescence to understand if there is an internalization inside the cells of this PS and their cellular localization.

One of the most important characteristics of PS in PDT, is to be non-toxic until activation by light. After internalization of both PS, the toxicity in darkness was evaluated. To evaluate the cell viability, MTT colorimetric assay was performed, 24 h after the treatment. As expected, **$H_2TPPF_{16}(SGlc)_4$** and **$ZnTPPF_{16}(SGlc)_4$** did not induce cell death in the darkness with the incubation concentration up to 10 μM and uptake time up to 4 h. These results allow us to pursue our study, evaluating the PDT effect of both glycoPSs on ARPE-19 cells.

The cell viability was assessed with the same, MTT colorimetric assay, 24 h after irradiation. Contrary to the results in darkness, and as expected, the incubation with **$H_2TPPF_{16}(SGlc)_4$** and **$ZnTPPF_{16}(SGlc)_4$** followed by PDT treatment during 40 min resulted in a decrease of cellular viability in a concentration- and time-

dependent manner. The obtained results for both PS were really similar and the only differences was in the incubation of 10 μM of **$H_2TPPF_{16}(SGlc)_4$** during 0.5 h, resulting in a higher decrease in cell viability when compared with **$ZnTPPF_{16}(SGlc)_4$**. Besides of that, 1.25 μM of **$ZnTPPF_{16}(SGlc)_4$** during 4 h of uptake induced a higher phototoxicity compared to **$H_2TPPF_{16}(SGlc)_4$** in the same conditions.

Once, MTT colorimetric assay, as explained before, is based on mitochondrial enzyme succinate dehydrogenase activity, another assay was performed to evaluate cellular viability in order to confirm the toxicity induced by both compounds. Twenty-four hours after the photodynamic assays, the trypan blue assay was performed. As expected, in the absence of light, the incubation of each compound during 2 h and the concentration described did not induce cell death. However, after PDT treatment, we found similar results of those obtained in MTT colorimetric assay for both compounds.

Once the effect of PDT was dependent of reactive oxygen species generation, their levels after PDT treatment with **$H_2TPPF_{16}(SGlc)_4$** and **$ZnTPPF_{16}(SGlc)_4$** were evaluated. Both compounds showed a significant increase in levels of ROS, mainly in anion superoxide levels, as revealed by the oxidation of DHE probe. Comparing both compounds, it is possible to note a higher level of ROS with **$ZnTPPF_{16}(SGlc)_4$** treatment. Taking into account the properties of transition metal in PSs, this increase was expected.

Based on the higher uptake and levels of ROS production by **$ZnTPPF_{16}(SGlc)_4$**, one could expect a higher toxicity of this compound. However, neither MTT colorimetric assay nor trypan blue assay revealed that. Besides the uptake by cells, PS subcellular localization have a dramatic impact for their biological effect, and consequently, PDT efficacy. ROS have a short half-life and they act to their site of generation or in its vicinity, so a subcellular of PS play a key role in PDT effect.[62, 88]

Drugs can be delivered into several organelles of the cell, such as cytosol, lysosome, nucleus and mitochondria. Depending on the subcellular localization of the PS, the cellular death after is photoactivation can be mediated by apoptosis, necrosis and/or autophagy. It was described that PSs localized in mitochondria are able to induce apoptosis very rapidly and with effectiveness. However, lysosomal or plasma membrane localization of the PS can also, initiate apoptosis and necrosis. The same study that described the high interaction of zinc with cellular membrane, in HeLa cells, reveals that zinc insertion in porphyrins lead to a decrease in the interaction with mitochondria.[117] Besides that, the authors found a higher PDT efficiency with zinc-porphyrins, suggesting a higher photodynamic efficiency directly proportional to membrane binding and not totally related to mitochondria accumulation. Moreover, the PDT effect also depends on the cells used. In the present work, the subcellular localization of both PSs was not assessed.

Chapter V
Conclusion and future perspectives

5.1 Conclusion and future perspectives

In this study, we intended to evaluate the photodynamic effect of two bioconjugated PSs: a free-porphyrin **($H_2TPPF_{16}(SGlc)_4$)** and a zinc-porphyrin **($ZnTPPF_{16}(SGlc)_4$)**, both with four thioglucose units. The presence of glucose in both PSs have a dual advantage in increasing aqueous solubility and improving lesions targeting in AMD, such as fibrosis and CNV. **$H_2TPPF_{16}(SGlc)_4$)** and **$ZnTPPF_{16}(SGlc)_4$** are decorated with four molecules of thioglucose, which can be recognized by Gal-1 overexpressed in subretinal fibrosis and which is known to be involved in the development of CNV in AMD. The inclusion of zinc(II) was to enhance the physicochemical properties to the free-base glycoderivative, and consequently the PDT effectiveness, since the presence of certain metals, such Zn, have the capacity of enhance ISC.

In order to mimic the EMT in RPE cells and subretinal fibrosis, we performed the *in vitro* photodynamic assays in ARPE-19 cell line, that under specific conditions present a mesenchymal spindle-shaped morphology, expressing a-SMA.

The uptake of **$ZnTPPF_{16}(SGlc)_4$** was slight higher in ARPE-19 cells than **$H_2TPPF_{16}(SGlc)_4$**, what can be due to a complexing effect of zinc with phosphate groups in cellular membrane.

In ARPE-19 cells, both PSs were non-toxic in darkness and the cytototoxicity after PDT was similar for both compounds. The PDT with **$ZnTPPF_{16}(SGlc)_4$** presented higher levels of ROS, namely anion superoxide, compared to **$H_2TPPF_{16}(SGlc)_4$**. Although the higher production of ROS, only a slight increase in phototoxicity after PDT with **$ZnTPPF_{16}(SGlc)_4$**, was observed compared to **$H_2TPPF_{16}(SGlc)_4$**.

Although both PSs were phototoxic against ARPE-19 cells with morphology reminiscent of fibroblasts, probably the cells were in a partial EMT state. We plan to confirm these data by inducing EMT with the transforming growth factor 1 (TGF-β1).

Once Gal-1 is described as a pro-angiogenic factor, and being involved in CNV development in the neovascular form of AMD, we also plan to test these promising PSs against CNV in a near future. Once there is no treatment for subretinal fibrosis, and taking account the adverse effects of available treatments, PDT with this type of PSs seems to be a promising therapeutic approach, for subretinal fibrosis, and eventually, CNV in neovascular AMD.

References

(1) Ansari, M. W.; Nadeem, A. Transparent Structures of the Eyeball Cornea, Lens, and Vitreous. In *Atlas of Ocular Anatomy*; 2016; pp 65–70. https://doi.org/10.1007/978-3-319-42781-2.

(2) Irsch, K.; Guyton, D. L. Anatomy of Eyes BT - Encyclopedia of Biometrics; Li, S. Z., Jain, A., Eds.; Springer US: Boston, MA, 2009; pp 11–16. https://doi.org/10.1007/978-0-387-73003-5_253.

(3) Joyce C, Le PH, S. N. Histology, Retina. https://www.ncbi.nlm.nih.gov/books/NBK546692 (accessed Aug 10, 2020).

(4) Campbell, M.; Humphries, P. The Blood-Retina Barrier: Tight Junctions and Barrier Modulation. *Adv. Exp. Med. Biol.* **2012**, *763*, 70–84.

(5) Bhutto, I.; Lutty, G. Understanding Age-Related Macular Degeneration (AMD): Relationships between the Photoreceptor/Retinal Pigment Epithelium/Bruch's Membrane/Choriocapillaris Complex. *Mol. Aspects Med.* **2012**, *33* (4), 295–317. https://doi.org/10.1016/j.mam.2012.04.005.

(6) Strauss, O. The Retinal Pigment Epithelium in Visual Function. *Physiol. Rev.* **2005**, *85* (3), 845–881. https://doi.org/10.1152/physrev.00021.2004.

(7) Curcio, C. A.; Johnson, M. *Structure, Function, and Pathology of Bruch's Membrane*, Fifth Edit.; Elsevier Inc., 2012; Vol. 146. https://doi.org/10.1016/B978-1-4557-0737-9.00020-5.

(8) Ford, K.; Amore, P. A. D.; Eye, S. Retinal Pigment Epithelial – Choroid Interactions. **2010**, 81–88.

(9) Gheorghe, A.; Mahdi, L.; Musat, O. AGE-RELATED MACULAR DEGENERATION. **2015**, *59* (2), 74–77.

(10) Gehrs, K. M.; Anderson, D. O. N. H.; Johnson, L. V; Hageman, G. S. Age-Related Macular Degeneration — Emerging Pathogenetic and Therapeutic Concepts. **2006**, 450–471. https://doi.org/10.1080/07853890600946724.

(11) Miller, J. W.; Bagheri, S.; Vavvas, D. G.; Service, R.; Eye, M.; Medical, H. Advances in Age-Related Macular Degeneration Understanding and Therapy. **2017**, *10* (2), 119–130. https://doi.org/10.17925/USOR.2017.10.02.119.Advances.

(12) García-layana, A. Early and Intermediate Age-Related Macular Degeneration : Update and Clinical Review. **2017**, 1579–1587.

(13) Al-Zamil, W. M.; Yassin, S. A. Recent Developments in Age-Related Macular Degeneration: A Review. *Clin. Interv. Aging* **2017**, *12*, 1313–1330. https://doi.org/10.2147/CIA.S143508.

(14) Bourne, R. R. A.; Flaxman, S. R.; Braithwaite, T.; Cicinelli, M. V.; Das, A.; Jonas, J. B.; Keeffe, J.; Kempen, J.; Leasher, J.; Limburg, H.; Naidoo, K.; Pesudovs, K.; Resnikoff, S.; Silvester, A.; Stevens, G. A.; Tahhan, N.; Wong, T.; Taylor, H. R.; Ackland, P.; Arditi, A.; Barkana, Y.; Bozkurt, B.; Wormald, R.; Bron, A.; Budenz, D.; Cai, F.; Casson, R.; Chakravarthy, U.; Congdon, N.; Peto, T.; Choi, J.; Dana, R.; Palaiou, M.; Dandona, R.; Dandona, L.; Shen, T.; Dekaris, I.; Del Monte, M.; Deva, J.; Dreer, L.; Frazier, M.; Ellwein, L.; Hejtmancik, J.; Frick, K.; Friedman, D.; Javitt, J.; Munoz, B.; Quigley, H.; Ramulu, P.; Robin, A.; Tielsch, J.; West, S.; Furtado, J.; Gao, H.; Gazzard, G.; George, R.; Gichuhi, S.; Gonzalez, V.; Hammond, B.; Hartnett, M. E.; He, M.; Hirai, F.; Huang, J.; Ingram, A.; Joslin, C.; Khanna, R.; Stambolian, D.; Khairallah, M.; Kim, J.; Lambrou, G.; Lansingh, V. C.; Lanzetta, P.; Lim, J.; Mansouri, K.; Mathew, A.; Morse, A.; Musch, D.; Nangia, V.; Battaglia, M.; Yaacov, F.; Raju, M.; Rossetti, L.; Saaddine, J.; Sandar, M.; Serle, J.; Shetty, R.; Sieving, P.; Silva, J. C.; Sitorus, R. S.; Tejedor, J.; Tsilimbaris, M.; van Meurs, J.; Varma, R.; Virgili, G.; Volmink, J.; Xing, Y.; Wang, N. L.; Wiedemann, P.; Zheng, Y. Magnitude, Temporal Trends, and Projections of the Global Prevalence of Blindness and Distance and near Vision Impairment: A Systematic Review and Meta-Analysis. *Lancet Glob. Heal.* **2017**, *5* (9), e888–e897. https://doi.org/10.1016/S2214-109X(17)30293-0.

(15) Li, J. Q.; Welchowski, T.; Schmid, M.; Mauschitz, M. M.; Holz, F. G.; Finger, R. P. Prevalence and Incidence of Age-Related Macular Degeneration in Europe: A Systematic Review and Meta-Analysis. *Br. J. Ophthalmol.* **2019**, 1–8. https://doi.org/10.1136/bjophthalmol-2019-314422.

(16) Jonas, J. B.; Cheung, C. M. G.; Panda-Jonas, S. Updates on the Epidemiology of Age-Related Macular Degeneration. *Asia-Pacific J. Ophthalmol.* **2017**, *6* (6), 493–497. https://doi.org/10.22608/APO.2017251.

(17) Li, J. Q.; Welchowski, T.; Schmid, M.; Letow, J.; Wolpers, A. C.; Holz, F. G.; Finger, R. P. Retinal Diseases in Europe: Prevalence, Incidence and Healthcare Needs. *Euretina* **2017**, No. August.

(18) Shim, S. H.; Kim, S. G.; Bae, J. H.; Yu, H. G.; Song, S. J. Risk Factors for Progression of Early Age-

Related Macular Degeneration in Koreans. *Ophthalmic Epidemiol.* **2016**, *23* (2), 80–87. https://doi.org/10.3109/09286586.2015.1129425.

(19) X. Shaw, P.; Stiles, T.; Douglas, C.; Ho, D.; Fan, W.; Du, H.; Xiao, X. Oxidative Stress, Innate Immunity, and Age-Related Macular Degeneration. *AIMS Mol. Sci.* **2016**, *3* (2), 196–221. https://doi.org/10.3934/molsci.2016.2.196.

(20) Colijn, J. M.; Buitendijk, G. H. S.; Prokofyeva, E.; Alves, D.; Cachulo, M. L.; Khawaja, A. P.; Cougnard-Gregoire, A.; Merle, B. M. J.; Korb, C.; Erke, M. G.; Bron, A.; Anastasopoulos, E.; Meester-Smoor, M. A.; Segato, T.; Piermarocchi, S.; de Jong, P. T. V. M.; Vingerling, J. R.; Topouzis, F.; Creuzot-Garcher, C.; Bertelsen, G.; Pfeiffer, N.; Fletcher, A. E.; Foster, P. J.; Silva, R.; Korobelnik, J.-F.; Delcourt, C.; Klaver, C. C. W. Prevalence of Age-Related Macular Degeneration in Europe: The Past and the Future. *Ophthalmology* **2017**, *124* (12), 1753–1763. https://doi.org/10.1016/j.ophtha.2017.05.035.

(21) Salimiaghdam, N.; Riazi-Esfahani, M.; Fukuhara, P.; Schneider, K.; Kenney, C. Age-Related Macular Degeneration (AMD): A Review on Its Epidemiology and Risk Factors. *Open Ophthalmol. J.* **2019**, *13*, 90–99. https://doi.org/10.2174/1874364101913010090.

(22) Jong, J. R. V. A. H. D. E. G. P. T. V. M. de. Age-Related Macular Degeneration and Smoking. The Rotterdam Study. *Arch. Ophthalmol. (Chicago, Ill. 1960)* **1996**, *114* (10), 1193–1196. https://doi.org/10.1001/archopht.1996.01100140393005.

(23) Chalam, K. V.; Khetpal, V.; Rusovici, R.; Balaiya, S. A Review: Role of Ultraviolet Radiation in Age-Related Macular Degeneration. *Eye Contact Lens* **2011**, *37* (4), 225–232. https://doi.org/10.1097/ICL.0b013e31821fbd3e.

(24) Tokarz, P.; Kaarniranta, K.; Blasiak, J. Role of Antioxidant Enzymes and Small Molecular Weight Antioxidants in the Pathogenesis of Age-Related Macular Degeneration (AMD). *Biogerontology* **2013**, *14* (5), 461–482. https://doi.org/10.1007/s10522-013-9463-2.

(25) Fritsche, L. G.; Igl, W.; Bailey, J. N. C.; Grassmann, F.; Sengupta, S.; Bragg-Gresham, J. L.; Burdon, K. P.; Hebbring, S. J.; Wen, C.; Gorski, M.; Kim, I. K.; Cho, D.; Zack, D.; Souied, E.; Scholl, H. P. N.; Bala, E.; ELee, K.; Hunter, D. J.; Sardell, R. J.; Mitchell, P.; Merriam, J. E.; Cipriani, V.; Hoffman, J. D.; Schick, T.; Lechanteur, Y. T. E.; Guymer, R. H.; Johnson, M. P.; Jiang, Y.; Stanton, C. M.; Buitendijk, G. H. S.; Zhan, X.; Kwong, A. M.; Boleda, A.; Brooks, M.; Gieser, L.; Ratnapriya, R.; Branham, K. E.; Foerster, J. R.; Heckenlively, J. R.; Othman, M. I.; Vote, B. J.; Liang, H. H.; Souzeau, E.; McAllister, I. L.; Isaacs, T.; Hall, J.; Lake, S.; Mackey, D. A.; Constable, I. J.; Craig, J. E.; Kitchner, T. E.; Yang, Z.; Su, Z.; Luo, H.; Chen, D.; Ouyang, H.; Flagg, K.; Lin, D.; Mao, G.; Ferreyra, H.; Stark, K.; Von Strachwitz, C. N.; Wolf, A.; Brandl, C.; Rudolph, G.; Olden, M.; Morrison, M. A.; Morgan, D. J.; Schu, M.; Ahn, J.; Silvestri, G.; Tsironi, E. E.; Park, K. H.; Farrer, L. A.; Orlin, A.; Brucker, A.; Li, M.; Curcio, C. A.; Mohand-Sa'd, S.; Sahel, J. A.; Audo, I.; Benchaboune, M.; Cree, A. J.; Rennie, C. A.; Goverdhan, S. V.; Grunin, M.; Hagbi-Levi, S.; Campochiaro, P.; Katsanis, N.; Holz, F. G.; Blond, F.; Blanché, H.; Deleuze, J. F. ois; Igo, R. P.; Truitt, B.; Peachey, N. S.; Meuer, S. M.; Myers, C. E.; Moore, E. L.; Klein, R.; Hauser, M. A.; Postel, E. A.; Courtenay, M. D.; Schwartz, S. G.; Kovach, J. L.; Scott, W. K.; Liew, G.; Tan, A. G.; Gopinath, B.; Merriam, J. C.; Smith, R. T.; Khan, J. C.; Shahid, H.; Moore, A. T.; McGrath, J. A.; Laux, R.; Brantley, M. A.; Agarwal, A.; Ersoy, L.; Caramoy, A.; Langmann, T.; Saksens, N. T. M.; Jong, E. K.; Hoyng, C. B.; Cain, M. S.; Richardson, A. J.; Martin, T. M.; Blangero, J.; Weeks, D. E.; Dhillon, B.; Van Duijn, C. M.; Doheny, K. F.; Romm, J.; Klaver, C. C. W.; Hayward, C.; Gorin, M. B.; Klein, M. L.; Baird, P. N.; Den Hollander, A. I.; Fauser, S.; WYates, J. R.; Allikmets, R.; Wang, J. J.; Schaumberg, D. A.; Klein, B. E. K.; Hagstrom, S. A.; Chowers, I.; Lotery, A. J.; Léveillard, T.; Zhang, K.; Brilliant, M. H.; Hewitt, A. W.; Swaroop, A.; Chew, E. Y.; Pericak-Vance, M. A.; DeAngelis, M.; Stambolian, D.; Haines, J. L.; Iyengar, S. K.; Weber, B. H. F.; Abecasis, G. R.; Heid, I. M. A Large Genome-Wide Association Study of Age-Related Macular Degeneration Highlights Contributions of Rare and Common Variants. *Nat. Genet.* **2016**, *48* (2), 134–143. https://doi.org/10.1038/ng.3448.

(26) Ambati, J.; Fowler, B. J. Mechanisms of Age-Related Macular Degeneration. *Neuron* **2012**, *75* (1), 26–39. https://doi.org/10.1016/j.neuron.2012.06.018.

(27) Despotovic, I. N.; Ferrara, D. *6.1.2 - Geographic Atrophy*; Elsevier Inc., 2017; Vol. 121. https://doi.org/10.1016/B978-0-323-46121-4.00010-8.

(28) Miller, J. W.; Bagheri, S.; Vavvas, D. G. Advances in Age-Related Macular Degeneration Understanding and Therapy. *US ophthalmic Rev.* **2017**, *10* (2), 119–130. https://doi.org/10.17925/USOR.2017.10.02.119.

(29) Ishikawa, K.; Kannan, R.; Hinton, D. R. Molecular Mechanisms of Subretinal Fibrosis in Age-Related Macular Degeneration. *Exp. Eye Res.* **2016**, *142*, 19–25. https://doi.org/10.1016/j.exer.2015.03.009.
(30) Folkman, J. Angiogenesis: An Organizing Principle for Drug Discovery? *Nat. Rev. Drug Discov.* **2007**, *6* (4), 273–286. https://doi.org/10.1038/nrd2115.
(31) Cabral, T.; Mello, L. G. M.; Lima, L. H.; Polido, J.; Regatieri, C. V.; Belfort, R.; Mahajan, V. B. Retinal and Choroidal Angiogenesis: A Review of New Targets. *Int. J. Retin. Vitr.* **2017**, *3* (1), 1–13. https://doi.org/10.1186/s40942-017-0084-9.
(32) IMarkowska, A.; Cao, Z.; Panjwani, N. Glycobiology of Ocular Angiogenesis. *Glycobiology* **2014**, *24* (12), 1275–1282. https://doi.org/10.1093/glycob/cwu078.
(33) Shimada, C.; Xu, R.; Al-alem, L.; Stasenko, M.; Spriggs, D. R. Galectins and Ovarian Cancer. *Cancers (Basel).* **2020**, *12* (6), 1421. https://doi.org/10.3390/cancers12061421.
(34) Sundblad, V.; Mathieu, V.; Kiss, R.; Rabinovich, G. A. *Galectins : Key Players in the Tumor Microenvironment*, Second Edi.; Elsevier, 2013. https://doi.org/10.1016/B978-0-12-394296-8.00031-2.
(35) Argüeso, P.; Panjwani, N. Focus on Molecules: Galectin-3. *Exp. Eye Res.* **2008**, *92* (1), 2–3. https://doi.org/10.1038/jid.2014.371.
(36) Wu, D.; Kanda, A.; Liu, Y.; Kase, S.; Noda, K.; Ishida, S. Galectin-1 Promotes Choroidal Neovascularization and Subretinal Fibrosis Mediated via Epithelial-Mesenchymal Transition. *FASEB J. Off. Publ. Fed. Am. Soc. Exp. Biol.* **2019**, *33* (2), 2498–2513. https://doi.org/10.1096/fj.201801227R.
(37) Cousin, J. M.; Cloninger, M. J. The Role of Galectin-1 in Cancer Progression, and Synthetic Multivalent Systems for the Study of Galectin-1. *Int. J. Mol. Sci.* **2016**, *17* (9), 1566. https://doi.org/10.3390/ijms17091566.
(38) Kanda, A.; Noda, K.; Saito, W.; Ishida, S. Aflibercept Traps Galectin-1, an Angiogenic Factor Associated with Diabetic Retinopathy. *Sci. Rep.* **2015**, *5*, 17946. https://doi.org/10.1038/srep17946.
(39) Markowska, A. I.; Liu, F.-T.; Panjwani, N. Galectin-3 Is an Important Mediator of VEGF- and BFGF-Mediated Angiogenic Response. *J. Exp. Med.* **2010**, *207* (9), 1981–1993. https://doi.org/10.1084/jem.20090121.
(40) Yuan, X.; Gu, X.; Crabb, J. S.; Yue, X.; Shadrach, K.; Hollyfield, J. G.; Crabb, J. W. Quantitative Proteomics: Comparison of the Macular Bruch Membrane/Choroid Complex from Age-Related Macular Degeneration and Normal Eyes. *Mol. Cell. Proteomics* **2010**, *9* (6), 1031–1046. https://doi.org/10.1074/mcp.M900523-MCP200.
(41) Coleman, H. R.; Chan, C.; Iii, F. L. F.; Chew, E. Y. Age-Related Macular Degeneration. *Lancet* **2008**, *372* (9652), 1835–1845. https://doi.org/10.1016/S0140-6736(08)61759-6.
(42) Lim, L. S.; Mitchell, P.; Seddon, J. M.; Holz, F. G.; Wong, T. Y. Age-Related Macular Degeneration. *Lancet* **2012**, *379* (9827), 1728–1738. https://doi.org/10.1016/S0140-6736(12)60282-7.
(43) Group, A.-R. E. D. S. R. A Randomized, Placebo-Controlled, Clinical Trial of High-Dose Supplementation With Vitamins C and E, Beta Carotene, and Zinc for Age-Related Macular Degeneration and Vision Loss: AREDS Report No. 8. *Arch. Ophthalmol. (Chicago, Ill. 1960)* **2001**, *119* (10), 1417–1436. https://doi.org/10.1001/archopht.119.10.1417.
(44) Chew, E. Y.; Clemons, T. E.; Agrón, E.; Sperduto, R. D.; Sangiovanni, J. P.; Kurinij, N.; Davis, M. D. NIH Public AccessLong-Term Effects of Vitamins C, E, Beta-Carotene and Zinc on Age-Related Macular Degeneration. AREDS Report No. 35. *Ophthalmology* **2014**, *120* (8), 1604–1611. https://doi.org/10.1016/j.ophtha.2013.01.021.Long-Term.
(45) Virgili, G.; Bini, A. Laser Photocoagulation for Neovascular Age-Related Macular Degeneration. *Cochrane database Syst. Rev.* **2007**, No. 3, CD004763. https://doi.org/10.1002/14651858.CD004763.pub2.
(46) Campochiaro, P. A. Retinal and Choroidal Neovascularization. *J. Cell. Physiol.* **2000**, *184* (3), 301–310. https://doi.org/10.1002/1097-4652(200009)184:3<301::AID-JCP3>3.0.CO;2-H.
(47) Solomon, S. D.; Lindsley, K.; Vedula, S. S.; Krzystolik, M. G.; Hawkins, B. S. Anti-Vascular Endothelial Growth Factor for Neovascular Agerelated Macular Degeneration. *Cochrane Database Syst. Rev.* **2019**, *2019* (3). https://doi.org/10.1002/14651858.CD005139.pub4.
(48) Kim, R. Introduction, Mechanism of Action and Rationale for Anti-Vascular Endothelial Growth Factor Drugs in Age-Related Macular Degeneration. *Indian J. Ophthalmol.* **2007**, *55* (6), 413–415. https://doi.org/10.4103/0301-4738.36473.
(49) Cunningham, E. T.; Ph, D.; Feinsod, M. Pegaptanib for Neovascular Age-Related Macular

Degeneration. *N. Engl. J. Med.* **2004**, *351* (27), 2805–2816. https://doi.org/10.1056/NEJMoa042760.
(50) Kaiser, P. K.; Chung, C. Y.; Ph, D.; Kim, R. Y.; Study, M. Ranibizumab for Neovascular Age-Related Macular Degeneration Philip. *new J. Engl. Med.* **2006**, *355*, 1419–1431.
(51) Eandi, C. M.; Alovisi, C.; De Sanctis, U.; Grignolo, F. M. Treatment for Neovascular Age Related Macular Degeneration: The State of the Art. *Eur. J. Pharmacol.* **2016**, *787*, 78–83. https://doi.org/10.1016/j.ejphar.2016.03.002.
(52) Schwartzentruber, D. J.; Topalian, S. L.; Steinberg, S. M.; Ph, D.; Chen, H. X.; Rosenberg, S. A.; Ph, D. A Randomized Trial of Bevacizumab, an Anti–Vascular Endothelial Growth Factor Antibody, for Metastatic Renal Cancer. *N. Engl. J. Med.* **2003**, *349*, 427–434.
(53) Sarwar, S.; Clearfield, E.; Mk, S.; Ma, S.; Aj, B.; Hanout, M.; Agarwal, A.; Yj, S.; Dv, D. Aflibercept for Neovascular Age-Related Macular Degeneration. *Cochrane database Syst. Rev.* **2016**, No. 2, CD011346. https://doi.org/10.1002/14651858.CD011346.pub2.www.cochranelibrary.com.
(54) Zhang, M.; Yu, D.; Yang, C.; Xia, Q.; Li, W.; Liu, B.; Li, H. The Pharmacology Study of a New Recombinant Human VEGF Receptor-Fc Fusion Protein on Experimental Choroidal Neovascularization. *Pharm. Res.* **2009**, *26* (1), 204–210. https://doi.org/10.1007/s11095-008-9718-9.
(55) de Oliveira Dias, J. R.; de Andrade, G. C.; Novais, E. A.; Farah, M. E.; Rodrigues, E. B. Fusion Proteins for Treatment of Retinal Diseases: Aflibercept, Ziv-Aflibercept, and Conbercept. *Int. J. Retin. Vitr.* **2016**, *2* (1), 3. https://doi.org/10.1186/s40942-016-0026-y.
(56) Zhang, M.; Zhang, J.; Yan, M.; Li, H.; Yang, C.; Yu, D. Recombinant Anti-Vascular Endothelial Growth Factor Fusion Protein Efficiently Suppresses Choridal Neovasularization in Monkeys. *Mol. Vis.* **2008**, *14*, 37–49.
(57) Nguyen, Q. D.; Das, A.; Do, D. V; Dugel, P. U.; Gomes, A.; Holz, F. G.; Koh, A.; Pan, C. K.; Sepah, Y. J.; Patel, N.; MacLeod, H.; Maurer, P. Brolucizumab: Evolution through Preclinical and Clinical Studies and the Implications for the Management of Neovascular Age-Related Macular Degeneration. *Ophthalmology* **2020**, *127* (7), 963–976. https://doi.org/https://doi.org/10.1016/j.ophtha.2019.12.031.
(58) Natalie Huang, P. O. Emerging Treatments for Neovascular AMD. *Retin. today* **2019**, No. June, 85–88. https://doi.org/10.1201/9781315146454-11.
(59) Falavarjani, K. G.; Nguyen, Q. D. Adverse Events and Complications Associated with Intravitreal Injection of Anti-VEGF Agents : A Review of Literature. *Eye* **2013**, 1–8. https://doi.org/10.1038/eye.2013.107.
(60) Costagliola, C.; Morescalchi, F.; Duse, S.; Romano, D.; Mazza, G.; Parmeggiani, F.; Bartollino, S.; Semeraro, F. Systemic Thromboembolic Adverse Events in Patients Treated with Intravitreal Anti-VEGF Drugs for Neovascular Age-Related Macular Degeneration: An Update. *Expert Opin. Drug Saf.* **2019**, *18* (9), 803–815. https://doi.org/10.1080/14740338.2019.1643838.
(61) Sun, S. Y. J. Z. X. Resistance to Anti-VEGF Therapy in Neovascular Age-Related Macular Degeneration : A Comprehensive Review. *Drug Des. Devel. Ther.* **2016**, *10*, 1857–1867. https://doi.org/10.2147/DDDT.S97653.
(62) Patrícia M. R. Pereira, J. P. C. T. and R. F. Molecular Targeted Photodynamic Therapy for Cancer. In *The Handbook of Porphyrin Science*; World Scientific Publishing Company, 2016; Vol. Volume 39, pp 127–169. https://doi.org/10.1158/2159-8290.CD-14-0477.Universes.
(63) Avci, P.; Erdem, S.; Hamblin, M. Photodynamic Therapy: One Step Ahead with Self-Assembled Nanoparticles. *J. Biomed. Nanotechnol.* **2015**, *10*. https://doi.org/10.1166/jbn.2014.1953.
(64) HIL, M. D. D. A. J. s. History of Photodynamic Therapy. *Aust. N. Z. J. Surg.* **1991**, *61* (5), 340–348. https://doi.org/10.1111/j.1445-2197.1991.tb00230.x.
(65) Ormond, A. B.; Freeman, H. S. Dye Sensitizers for Photodynamic Therapy. *Materials (Basel).* **2013**, *6*, 817–840. https://doi.org/10.3390/ma6030817.
(66) Kessel, D. Photodynamic Therapy : A Brief History. *J. Clin. Med. Rev.* **2019**, *8*, 1581. https://doi.org/10.3390/jcm8101581.
(67) Pass, H. I. Photodynamic Therapy in Oncology: Mechanisms and Clinical Use. *J. Natl. Cancer Inst.* **1993**, *85* (6), 443–456. https://doi.org/10.1093/jnci/85.6.443.
(68) Kessel, D. Photodynamic Therapy : A Brief History. *J. Clin. Med. Rev.* **2019**, *8*, 1528. https://doi.org/10.3390/jcm8101581.
(69) Richard L.Lipson, Edward J.Baldes, A. M. O. Hematoporphyrin Derivative: A New Aid for Endoscopic Detection of Malignant Disease. *Am. Assoc. Thorac. Surg.* **1961**, *42* (5), 623–629.

https://doi.org/10.1016/S0022-5223(19)32560-7.
(70) Dougherty, Thomas JDougherty, T.; Gomer, C.; Weishaupt, K. Energetics and Efficiency of Photoinactivation of Murine Tumor Cells Containing Hematoporphyrin. *Cancer Res.* **1976**, *36* (August), 2330–2333.
(71) Dougherty, T. J.; Gomer, C. J.; Henderson, B. W.; Jori, G.; Kessel, D.; Korbelik, M.; Moan, J.; Peng, Q. Photodynamic Therapy. *J. Natl. Cancer Inst.* **1998**, *90* (12), 889–905. https://doi.org/10.1093/jnci/90.12.889.
(72) Battaglia, M.; Carlo, P.; Spina, L.; Berchicci, L.; Petruzzi, G.; Bandello, F. Photosensitizers and Photodynamic Therapy : Verteporfin. *Drugs Mech. Retin. Dis.* **2016**, *55*, 330–336. https://doi.org/10.1159/000434704.
(73) Robertson, C. A.; Evans, D. H.; Abrahamse, H. Photodynamic Therapy (PDT): A Short Review on Cellular Mechanisms and Cancer Research Applications for PDT. *J. Photochem. Photobiol. B Biol.* **2009**, *96* (1), 1–8. https://doi.org/10.1016/j.jphotobiol.2009.04.001.
(74) Kwiatkowski, S.; Knap, B.; Przystupski, D.; Saczko, J.; Kędzierska, E.; Knap-Czop, K.; Kotlińska, J.; Michel, O.; Kotowski, K.; Kulbacka, J. Photodynamic Therapy – Mechanisms, Photosensitizers and Combinations. *Biomed. Pharmacother.* **2018**, *106* (June), 1098–1107. https://doi.org/10.1016/j.biopha.2018.07.049.
(75) Dayer, M. R.; Moosavi-Movahedi, A. A.; Dayer, M. S. Band Assignment in Hemoglobin Porphyrin Ring Spectrum: Using Four-Orbital Model of Gouterman. *Protein Pept. Lett.* **2010**, *17* (4), 473–479. https://doi.org/10.2174/092986610790963645.
(76) Macdonald, I. A. N. J.; Dougherty, T. J. Basic Principles of Photodynamic Therapy. *J. Porphyr. Phthalocyanines* **2008**, No. 5, 105–129.
(77) De Rosa, F. S.; Bentley, M. V. L. B. Photodynamic Therapy of Skin Cancers: Sensitizers, Clinical Studies and Future Directives. *Pharm. Res.* **2000**, *17* (12), 1447–1455. https://doi.org/10.1023/A:1007612905378.
(78) De Freitas, L. F.; Hamblin, M. R. *Antimicrobial Photoinactivation with Functionalized Fullerenes*; Elsevier Inc., 2016. https://doi.org/10.1016/B978-0-323-42864-4.00001-4.
(79) Figueira, F.; Pereira, P. M. R.; Silva, S.; Cavaleiro, J. A. S.; Tomé, J. P. C. Porphyrins and Phthalocyanines Decorated with Dendrimers : Synthesis and Biomedical Applications. *Curr. Org. Synth.* **2014**, No. 11, 110–126. https://doi.org/10.1002/chin.201440270.
(80) Chilakamarthi, U.; Giribabu, L. Photodynamic Therapy: Past, Present and Future. *Chem. Rec.* **2017**, *17* (8), 775–802. https://doi.org/10.1002/tcr.201600121.
(81) Bispo, M.; Pereira, P. M. R.; Setaro, F.; Rodríguez-Morgade, M. S.; Fernandes, R.; Torres, T.; Tomé, J. P. C. A Galactose Dendritic Silicon (IV) Phthalocyanine as a Photosensitizing Agent in Cancer Photodynamic Therapy. *Chempluschem* **2018**, *83* (9), 855–860. https://doi.org/10.1002/cplu.201800370.
(82) Pereira, P. M. R.; Silva, S.; Cavaleiro, J. A. S.; Ribeiro, C. A. F.; Tomé, J. P. C.; Fernandes, R. Galactodendritic Phthalocyanine Targets Carbohydrate-Binding Proteins Enhancing Photodynamic Therapy. *PLoS One* **2014**, *9* (4), 22–30. https://doi.org/10.1371/journal.pone.0095529.
(83) Pereira, P. M. R.; Silva, S.; Ramalho, J. S.; Gomes, C. M.; Girão, H.; Cavaleiro, J. A. S.; Ribeiro, C. A. F.; Tomé, J. P. C.; Fernandes, R. The Role of Galectin-1 in *in Vitro* and *in Vivo* Photodynamic Therapy with a Galactodendritic Porphyrin. *Eur. J. Cancer* **2016**, *68*, 60–69. https://doi.org/10.1016/j.ejca.2016.08.018.
(84) Calvaresi, E. C.; Hergenrother, P. J. Glucose Conjugation for the Specific Targeting and Treatment of Cancer. *Chem. Sci.* **2013**, *4* (6), 2319–2333. https://doi.org/10.1039/C3SC22205E.
(85) Brancaleon, L.; Moseley, H. Laser and Non-Laser Light Sources for Photodynamic Therapy. *Lasers Med. Sci.* **2002**, *17* (3), 173–186. https://doi.org/10.1007/s101030200027.
(86) Kim, M. M.; Darafsheh, A. Light Sources and Dosimetry Techniques for Photodynamic Therapy. *Photochem. Photobiol.* **2020**, *96*, 280–294. https://doi.org/10.1111/php.13219.
(87) Breskey, J. D.; Lacey, S. E.; Vesper, B. J.; Paradise, W. A.; Radosevich, J. A.; Colvard, M. D. Photodynamic Therapy: Occupational Hazards and Preventative Recommendations for Clinical Administration by Healthcare Providers. *Photomed. Laser Surg.* **2013**, *31* (8), 398–407. https://doi.org/10.1089/pho.2013.3496.
(88) Castano, A. P.; Demidova, T. N.; Hamblin, M. R. Mechanisms in Photodynamic Therapy: Part One-Photosensitizers, Photochemistry and Cellular Localization. *Photodiagnosis Photodyn. Ther.* **2014**, *1* (4),

279–293. https://doi.org/10.1016/S1572-1000(05)00007-4.Mechanisms.
(89) Plaetzer, K.; Krammer, B.; Berlanda, J.; Berr, F. Photophysics and Photochemistry of Photodynamic Therapy: Fundamental Aspects. *Lasers Med. Sci.* **2009**, *24* (2), 259–268. https://doi.org/10.1007/s10103-008-0539-1.
(90) Huang, Z. A Review of Progress in Clinical Photodynamic Therapy. *Technol. Cancer Res. Treat.* **2005**, *4* (3), 283–293. https://doi.org/10.1177/153303460500400308.
(91) Wormald, R.; Evans, J. R.; Smeeth, L. L.; Henshaw, K. S. Photodynamic Therapy for Neovascular Age-related Macular Degeneration. *Cochrane Database Syst. Rev.* **2005**, No. 3. https://doi.org/10.1002/14651858.CD002030.pub3.
(92) Scott, L. J.; Goa, K. L. Verteporfin. *Drug Aging* **2000**, *16* (2), 139–146. https://doi.org/10.2165/00002512-200016020-00005.
(93) Ammar, D. A.; Kahook, M. Y. In Vitro Effects of Verteporfn on Ocular Cells. *Mol. Vis.* **2013**, *19*, 424–429.
(94) Visudyne (Verteporfin for Injection). 2000.
(95) Schmidt-erfurth, U.; Laqua, H.; Zografos, L.; Strong, A.; Lane, A. M.; Bressler, N. M. Photodynamic Therapy of Subfoveal Choroidal Neovascularization : Clinical and Angiographic Examples. *Graefe's Arch. Clin. Exp. Ophthalmol.* **1998**, *236* (5), 365–374.
(96) Sciences, C. Photodynamic Therapy of Subfoveal Choroidal Neovascularization in Age-Related Macular Degeneration With Verteporfin. *Arch. Ophthalmol. (Chicago, Ill. 1960)* **1999**, *117* (10), 1329–1345.
(97) Gao, Y.; Yu, T.; Zhang, Y.; Dang, G. Anti-VEGF Monotherapy Versus Photodynamic Therapy and Anti-VEGF Combination Treatment for Neovascular Age-Related Macular Degeneration: A Meta-Analysis. *Invest. Ophthalmol. Vis. Sci.* **2018**, *59* (10), 4307–4317. https://doi.org/10.1167/iovs.17-23747.
(98) Lazic, R.; Gabric, N. Verteporfin Therapy and Intravitreal Bevacizumab Combined and Alone in Choroidal Neovascularization Due to Age-Related Macular Degeneration. *Ophthalmology* **2007**, *114* (6), 1179–1185. https://doi.org/10.1016/j.ophtha.2007.03.006.
(99) Miller, J. W.; Le Couter, J.; Strauss, E. C.; Ferrara, N. Vascular Endothelial Growth Factor a in Intraocular Vascular Disease. *Ophthalmology* **2013**, *120* (1), 106–114. https://doi.org/10.1016/j.ophtha.2012.07.038.
(100) Afzal, A.; Shaw, L. C.; Ljubimov, A. V; Boulton, M. E.; Segal, M. S.; Grant, M. B. Retinal and Choroidal Microangiopathies: Therapeutic Opportunities. *Microvasc. Res.* **2007**, *74* (2–3), 131–144. https://doi.org/10.1016/j.mvr.2007.04.011.
(101) Mahmood, T.; Yang, P.-C. Western Blot: Technique, Theory, and Trouble Shooting. *N. Am. J. Med. Sci.* **2012**, *4* (9), 429–434. https://doi.org/10.4103/1947-2714.100998.
(102) Walker, J. M. The Bicinchoninic Acid (BCA) Assay for Protein Quantitation. **2009**.
(103) Colorimetric, B.; Assays, P.; Präbst, K.; Engelhardt, H.; Ringgeler, S. Chapter 1. *1601*, 1–17. https://doi.org/10.1007/978-1-4939-6960-9.
(104) Strober, W. Trypan Blue Exclusion Test of Cell Viability. *Curr. Protoc. Immunol.* **2015**, *111*, A3.B.1-A3.B.3. https://doi.org/10.1002/0471142735.ima03bs111.
(105) Josefsen, L. B.; Boyle, R. W. Photodynamic Therapy and the Development of Metal-Based Photosensitisers. *Met. Based. Drugs* **2008**, *2008*, 276109. https://doi.org/10.1155/2008/276109.
(106) Pereira, P. M. R.; Silva, S.; Ramalho, J. S.; Gomes, C. M.; Girão, H.; Cavaleiro, J. A. S.; Ribeiro, C. A. F.; Tomé, J. P. C.; Fernandes, R. The Role of Galectin-1 in *in Vitro* and *in Vivo* Photodynamic Therapy with a Galactodendritic Porphyrin. *Eur. J. Cancer* **2016**, *68*, 60–69. https://doi.org/https://doi.org/10.1016/j.ejca.2016.08.018.
(107) Lin, Y.; Zhou, T.; Bai, R.; Xie, Y. Chemical Approaches for the Enhancement of Porphyrin Skeleton-Based Photodynamic Therapy. *J. Enzyme Inhib. Med. Chem.* **2020**, *35* (1), 1080–1099. https://doi.org/10.1080/14756366.2020.1755669.
(108) Huang, Q.; Pan, Z.; Wang, P.; Chen, Z.; Zhang, X.; Xu, H. Zinc(II) and Copper(II) Complexes of β-Substituted Hydroxylporphyrins as Tumor Photosensitizers. *Bioorg. Med. Chem. Lett.* **2006**, *16* (11), 3030–3033. https://doi.org/https://doi.org/10.1016/j.bmcl.2005.02.094.
(109) Marydasan, B.; Nair, A. K.; Ramaiah, D. Optimization of Triplet Excited State and Singlet Oxygen Quantum Yields of Picolylamine–Porphyrin Conjugates through Zinc Insertion. *J. Phys. Chem. B* **2013**, *117* (43), 13515–13522. https://doi.org/10.1021/jp407524w.
(110) Hwang, J. C.; Del Priore, L. V; Freund, K. B.; Chang, S.; Iranmanesh, R. Development of Subretinal

Fibrosis after Anti-VEGF Treatment in Neovascular Age-Related Macular Degeneration. *Ophthalmic surgery, lasers imaging Off. J. Int. Soc. Imaging Eye* **2011**, *42* (1), 6–11. https://doi.org/10.3928/15428877-20100924-01.

(111) Wynn, T. A. Common and Unique Mechanisms Regulate Fibrosis in Various Fibroproliferative Diseases. *J. Clin. Invest.* **2007**, *117* (3), 524–529. https://doi.org/10.1172/JCI31487.

(112) Kalluri, R.; Weinberg, R. A. The Basics of Epithelial-Mesenchymal Transition. *J. Clin. Invest.* **2009**, *119* (6), 1420–1428. https://doi.org/10.1172/JCI39104.

(113) Tamiya, S.; Liu, L.; Kaplan, H. J. Epithelial-Mesenchymal Transition and Proliferation of Retinal Pigment Epithelial Cells Initiated upon Loss of Cell-Cell Contact. *Invest. Ophthalmol. Vis. Sci.* **2010**, *51* (5), 2755–2763. https://doi.org/10.1167/iovs.09-4725.

(114) Wu, D.; Kanda, A.; Liu, Y.; Kase, S.; Noda, K.; Ishida, S. Galectin-1 Promotes Choroidal Neovascularization and Subretinal Fibrosis Mediated via Epithelial- Mesenchymal Transition. *FASEB J.* **2019**, *33* (2), 2498–2513. https://doi.org/10.1096/fj.201801227R.

(115) Samuel, W.; Jaworski, C.; Postnikova, O. A.; Kutty, R. K.; Duncan, T.; Tan, L. X.; Poliakov, E.; Lakkaraju, A.; Redmond, T. M. Appropriately Differentiated ARPE-19 Cells Regain Phenotype and Gene Expression Profiles Similar to Those of Native RPE Cells. *Mol. Vis.* **2017**, *23*, 60–89.

(116) Leung, K. W.; Liu, M.; Xu, X.; Seiler, M. J.; Barnstable, C. J.; Tombran-Tink, J. Expression of ZnT and ZIP Zinc Transporters in the Human RPE and Their Regulation by Neurotrophic Factors. *Invest. Ophthalmol. Vis. Sci.* **2008**, *49* (3), 1221–1231. https://doi.org/10.1167/iovs.07-0781.

(117) Pavani, C.; Uchoa, A.; Oliveira, C.; Iamamoto, Y.; Baptista, M. Effect of Zinc Insertion and Hydrophobicity on the Membrane Interactions and PDT Activity of Porphyrin Photosensitizers. *Photochem. Photobiol. Sci.* **2009**, *8*, 233–240. https://doi.org/10.1039/b810313e.